Dynamic Modelling, Analysis, and Design Optimisation of a Pendulum-Coupled Tuned Mass Damper System Compared to a Multiple Tuned Mass Damper System on a Skyscraper: Case Study of the Taipei 101 Building

Ruben Peters

Bachelor Advanced Technology - University of Twente

July 29, 2024

Abstract—In this research project, the vibration mitigation performance of a multiple pendulum tuned mass damper (MTMD) system is evaluated and compared to the vibration mitigation performance of a single pendulum tuned mass damper (TMD) system. Two steel truss models of the Taipei 101 building are constructed, including the TMD and MTMD systems, using the finite element method (FEM). The dynamic behaviour of both systems is compared through numerical analysis based on suppression ability, robustness, space usage and off-tuning mitigation. The systems are assessed for various fundamental natural frequencies of the building in the models to simulate the short- and long-term off-tuning of the building frequency. It is found that the single TMD system which is currently installed in the Taipei 101 building performs more efficiently than the proposed MTMD system, based on the mentioned comparison methods. The difference by which the single TMD system outperforms the MTMD system is small for both the correctly tuned and the off-tuned fundamental natural frequencies of the building, although the suppression ability of both systems equally improves when the systems are tuned to the correct frequency. However, since the single TMD system requires less space and less materials, the single TMD system is more appropriate than the proposed MTMD system. The results provide insight in the behaviour of TMD and MTMD systems in general and are relevant for further comparison studies between these systems, for implementation in wind-excited structures.

Keywords: Vibration mitigation; TMD; MTMD; Truss FEM model; Robustness; Space usage; Off-tuning mitigation

I. INTRODUCTION

Buildings are becoming increasingly taller all around the modern world, because of the rise of innovative building techniques. Tall buildings are inherently more vulnerable to vibrations or dynamic excitation due to external forces that result from wind gusts or seismic activity, which could lead to fatigue or failure in the worse case, but also discomfort for building residents, caused by motion sickness. Therefore, this vulnerability of tall buildings to dynamic response should be mitigated. One method of suppressing the vibrations of a building induced by external forces is by using a tuned mass damper (TMD) system. This system consists of a mass which is attached to a spring and a damper, for which the system parameters are tuned such that the building vibrations are opposed by the movement of the TMD system. This suppresses the vibrations of the building, which keeps the dynamic response of the building to a minimum.

The use of TMD systems[1][2][3][4][5][6] in buildings and the optimal design of these systems has been researched in detail in the past. There exist multiple types of TMD systems, for example the conventional passive TMD system, where the oscillation of a big mass (building) is suppressed by the oscillation of a smaller mass (TMD system mass), without adding any energy to the system to control it in any way. This system is self-stabilising, which makes it a sustainable solution for building stabilisation. The use of active[7][8] or semi-active[9] TMD systems has been investigated as well. An active TMD system uses a small mass that is driven by control inputs to counter vibrations of a big mass and a semi-active TMD system consist of a passive TMD system, of which the system parameters can be altered by for example applying control on the damping or the stiffness of the system. These systems provide the opportunity to modify the behaviour of a TMD system based on the natural frequency[10][11] of the building, which might change under weather circumstances, due to changing external forces or due to structural changes over time. This results in more effective vibration control with respect to the passive TMD system in most cases. However, the necessity of energy supply for controlling these systems, makes them less efficient and less sustainable.

Another method that ensures that a TMD system can be operational within a frequency bandwidth instead of one specific tuning frequency, is to use multiple tuned mass dampers[12][13][14][15][16][17][18][19][20] in one building. The multiple TMDs will all be tuned to a slightly different frequency around the natural frequency of the building, which means that this system provides robustness against temporary changes in natural frequency of the building, but also against long term changes due to changes in structure or geography of and around the building. This prevention of off-tuning can be essential for the TMD system to stay effective in vibration suppression over time. Additionally, the advantage of a multiple tuned mass damper (MTMD) system, is that it can be implemented using passive TMDs, while still resulting in a robust system which can operate for a range of frequencies.

More recent research consists of the use of inerters[21][22][23]

in combination with TMD systems. These inerters provide improved damping and behave as a 'virtual mass'. This means that using inerters results in better building vibration mitigation, especially when the inerter system spans multiple floors[24][25][26] of the building. This is the case because the acceleration between the locations where the inerter is attached becomes larger when the inerter spans more floors, which causes the inerter to have a larger effect on the vibration mitigation.

Furthermore, specific research has been done into the dynamic characteristics and the TMD system of the Taipei 101 building[10][27][28] (see figure 1), located in Taiwan, which is one of the tallest buildings in the world and currently uses the heaviest TMD system in the world. Based on collected data from field measurements[29][30] during typhoons and earthquakes, such as the Masta (2005) and Talim (2005) typhoons and the Wenchuan (2008) and Tohoku (2011) earthquakes, the performance of the TMD system in the Taipei 101 building was monitored. The measured acceleration and displacement signals can also be used for further tuning of the TMD system. It was found that little research has been done into the possibility of using a MTMD system for the Taipei 101 building specifically, despite the fact that such a system might have multiple advantages, such as more robustness due to the wider frequency operation bandwidth and the possibility of more efficient, distributed mass placement.

Fig. 1: Taipei 101 building[31]

This research project proposes the use of a MTMD system in the Taipei 101 building and evaluates the effectiveness of this system in comparison to the currently installed TMD system. The research question is: how can the TMD system in the Taipei 101 building be improved by using multiple smaller, distributed TMD systems (MTMD system) instead of one large TMD system? The method to solve this question will be numerical analysis. First, a simplified model will be made of the existing Taipei 101 building, using the finite element method (FEM), by deriving the equations of motion for the simplified building (using Euler-Bernoulli beam theory) along with the TMD system. The vibration suppression abilities of the design will be studied via simulation in MATLAB. Subsequently, the model will be modified to a MTMD system and the suppression abilities of the new design will be studied. Appropriate wind models (based on measured data) will be used to simulate the building displacement among other dynamic properties. The building displacement will be determined along the height of the building, for the cases without the TMD system, with the TMD system and with the MTMD system. For both TMD systems, parameter optimisation will be performed by applying the most appropriate optimisation procedure. In the end, a comparison will be performed which ultimately leads to conclusions about the best possible TMD system for this building in terms of suppression ability, off-tuning mitigation, robustness and efficiency in terms of space usage.

II. THEORETICAL BACKGROUND

In this section, an overview is provided of the theoretical knowledge which is required to understand the numerical model of the building. Various theoretical concepts are addressed in the subsections below.

First, the static building has to be modelled in MATLAB, by approximating the structure of the building as closely as possible. This will be done by using the finite element method, which will be explained in section II-A In order to make the static building move, forces are applied to the building which represent the wind force. This wind force causes the beams of the building to deflect, in the transverse and axial direction, which is explained in section II-B and II-C respectively. The pendulum tuned mass damper system is explained in section II-H and the Newmark-beta method, which is used to calculate the building motion over time, is explained in section II-I.

A. Finite element method model

Modelling the dynamic motion of a building in detail can be a complex task, which requires choices regarding the complexity of the building model in combination with the computational cost of a numerical simulation. For the dynamic model of the Taipei 101 building in this research project, a 2D finite element method (FEM) model is made in MATLAB. The finite element method is a numerical simulation method which allows for solving differential equations for complex structures or systems, by dividing the structure or system into multiple smaller elements. This allows to simulate the dynamic behaviour of large and complex structures over time.

In the case of a building, the differential equations that describe the building motion can be solved by dividing the building into many different sections, represented by beams in this research project. Each of the beam elements has two end points, which are called 'nodes' of the FEM model. These nodes are connection points, where multiple beams can be connected to. All of the forces, accelerations, velocities and

displacements that are calculated, are calculated for the nodes of the FEM model, which means that the nodes displace when a certain force is applied to them. All nodes of the building have 3 degrees of freedom, which will be discussed in section II-D. The single TMD building model will consist of 103 nodes, which means that the entire building configuration in this model will have a total of 309 degrees of freedom. How much the nodes displace depends on the properties of the beam elements which connect the nodes of the building.

The chosen beam configuration for the model is an I-beam, because I-beams are commonly used beams for which the moment of inertia is known. These I-beams are placed in the model to represent every wall and floor, such that every building floor is represented by a rectangular box. Within these rectangular boxes, two diagonal beam elements are placed, which ensures that all bending directions are accounted for. These I-beams are elaborated upon further in section II-E. The static truss FEM building model, including a single TMD system is shown in figure 24.

B. Transverse beam motion (Euler-Bernoulli beam theory)

Euler-Bernoulli beam theory is used to determine the transverse motion of the beam elements in the model. The book 'Structural Dynamics: An Introduction to Computer Methods'[32] from Roy R. Craig is used for the complete derivation of the global stiffness and mass matrices used in the model, that satisfy the Euler-Bernoulli equations. This derivation is shown in this and the following sections, namely sections II-B, II-C and II-D.

1) Assumptions

Euler-Bernoulli beam theory is based on some general assumptions, which are listed below.

- The axis that is perpendicular to the length of the beam does not extend or contract. This axis is called the neutral axis.
- The cross-sections of the beam which are perpendicular to the neutral axis always stay perpendicular to the neutral axis, also when the neutral axis deforms.
- The material behaves linearly and always is in the elastic range of the material.
- Shear stresses are neglected.
- The principle stresses act in the xy-plane (the xy-plane is a principal plane.

These assumptions are applied in the derivation of the Euler-Bernoulli equations and provide insight in how an Euler-Bernoulli beam behaves.

2) Assumed modes method and beam equations

The shape of a beam can be approximated by the assumed modes method. The displacement of a SDOF continuous beam can be approximated by the function

$$u(x,t) = \psi(x)u(t), \tag{1}$$

where $u(x,t)$ is the assumed mode of the system, $u(t)$ is the generalised displacement of the beam and $\psi(x)$ is the

shape function, which is any function that approximates the displacement of a deformed beam. In order to extend the assumed modes method to an N-DOF continuous system, N assumed mode functions are required, which is represented by

$$v(x,t) = \sum_{i=1}^{N} \psi_i(x)v_i(t). \tag{2}$$

Using Eq. (2), the transverse motion of a beam element of length L, density ρ, elasticity modulus E, cross-sectional area A and moment of inertia I can be computed. The shape functions of the beam should meet certain boundary conditions, which are

$$\begin{aligned}
\psi_1(0) &= 1, & \psi_1'(0) &= \psi_1(L) = \psi_1'(L) = 0, \\
\psi_2'(0) &= 1, & \psi_2(0) &= \psi_2(L) = \psi_2'(L) = 0, \\
\psi_3(L) &= 1, & \psi_3(0) &= \psi_3'(0) = \psi_3'(L) = 0, \\
\psi_4'(L) &= 1, & \psi_4(0) &= \psi_4'(0) = \psi_4(L) = 0.
\end{aligned} \tag{3}$$

Now, the general solution of Eq. (2) is equal to

$$v(x) = c_1 + c_2\left(\frac{x}{L}\right) + c_3\left(\frac{x}{L}\right)^2 + c_4\left(\frac{x}{L}\right)^3. \tag{4}$$

When filling in the boundary conditions shown in Eq. (3) into Eq. (4), four shape functions are obtained, which are

$$\begin{aligned}
\psi_1 &= 1 - 3\left(\frac{x}{L}\right)^2 + 2\left(\frac{x}{L}\right)^3, \\
\psi_2 &= x - 2L\left(\frac{x}{L}\right)^2 + L\left(\frac{x}{L}\right)^3, \\
\psi_3 &= 3\left(\frac{x}{L}\right)^2 - 2\left(\frac{x}{L}\right)^3, \\
\psi_4 &= -L\left(\frac{x}{L}\right)^2 + L\left(\frac{x}{L}\right)^3.
\end{aligned} \tag{5}$$

The stiffness and mass matrices of Euler-Bernoulli beams satisfy the equations

$$k_{ij} = \int_0^L EI\psi_i''\psi_j''dx \tag{6}$$

and

$$m_{ij} = \int_0^L \rho A\psi_i\psi_j dx, \tag{7}$$

respectively. Filling in the shape functions shown in Eq. (5) into Eqs. 6 and 7 gives the following stiffness and mass matrices:

$$\mathbf{k} = \left(\frac{EI}{L^3}\right)\begin{bmatrix} 12 & 6L & -12 & 6L \\ 6L & 4L^2 & -6L & 2L^2 \\ -12 & -6L & 12 & -6L \\ 6L & 2L^2 & -6L & 4L^2 \end{bmatrix} \tag{8}$$

$$\mathbf{m} = \left(\frac{\rho AL}{420}\right)\begin{bmatrix} 156 & 22L & 54 & -13L \\ 22L & 4L^2 & 13L & -3L^2 \\ 54 & 13L & 156 & -22L \\ -13L & -3L^2 & -22L & 4L^2 \end{bmatrix} \tag{9}$$

These stiffness and mass matrices can be used to calculate the transverse motion and the slope of the beam at the two nodes at the end of each beam element.

C. Axial beam motion

The axial motion of a beam element of length L, density ρ, elasticity modulus E and cross-sectional area A can also be computed using the assumed modes method discussed above. The formula

$$u(x,t) = \psi_1(x)u_1(t) + \psi_2(x)u_2(t) \qquad (10)$$

can be used for this. The boundary conditions that have to be satisfied for the axial motion are equal to

$$\begin{aligned}
\psi_1(0) &= 1, & \psi_1(L) &= 0, \\
\psi_2(0) &= 0, & \psi_2(L) &= 1.
\end{aligned} \qquad (11)$$

The general solution of Eq. (10) is equal to

$$u(x) = c_1 + c_2\left(\frac{x}{L}\right). \qquad (12)$$

Filling in the boundary conditions shown in Eq. (11) into Eq. (12) gives the shape functions

$$\psi_1(x) = 1 - \frac{x}{L}, \qquad \psi_2(x) = \frac{x}{L}. \qquad (13)$$

The stiffness and mass matrices for axial motion were found to satisfy the equations

$$k_{ij} = \int_0^L EA\psi_i'\psi_j'dx \qquad (14)$$

and

$$m_{ij} = \int_0^L \rho A\psi_i\psi_j dx, \qquad (15)$$

respectively. Filling in the shape functions shown in Eq. (13) into Eqs. (14) and (15) gives the following stiffness and mass matrices:

$$\mathbf{k} = \left(\frac{AE}{L}\right)\begin{bmatrix} 1 & -1 \\ -1 & 1 \end{bmatrix} \qquad (16)$$

$$\mathbf{m} = \left(\frac{\rho AL}{6}\right)\begin{bmatrix} 2 & 1 \\ 1 & 2 \end{bmatrix} \qquad (17)$$

These stiffness and mass matrices can be used to calculate the axial motion of the beam element at the two nodes at the end of each beam element.

D. Global building equations

Each node in the model will have 3 degrees of freedom, namely motion in the x-direction (transverse displacement), motion in the y-direction (axial displacement) and a change of motion in the x-direction (change in transverse displacement). For each node, a displacement in all of the degrees of freedom will be calculated, where the degrees of freedom will be represented as

$$\mathbf{u} = \begin{bmatrix} u_1 \\ u_2 \\ u_3 \end{bmatrix}, \qquad (18)$$

where u_1 will be the displacement in x-direction (transverse displacement), u_2 will be the displacement in y-direction (axial displacement) and u_3 will be the change of transverse displacement, which can also be explained as being the slope

of the beam at the nodes, with respect to the equilibrium position of the beam. The slope is denoted as

$$u_3 = \frac{du_1}{dy}, \qquad (19)$$

since the transverse displacement will be in x-direction because the building height will be parallel to the y-direction. This coordinate system will be explained in section II-D1.

In order to capture the behaviour of the beams for all of the degrees of freedom, the stiffness and mass matrices of the transverse and axial motion, which are found in Eqs. (8), (9), (16) and (17) should be combined into a single local stiffness and mass matrix, which can be used for each beam element. Then, these local stiffness and mass matrices should be combined to obtain a global stiffness and mass matrix, which represents the stiffness and mass of the entire building.

1) Global coordinate system
When considering a single beam element, a coordinate system can be assigned to the beam. E.g. the beam can be parallel to the x-axis, which makes movement in the y-direction transverse movement. Alternatively, the beam can be parallel to the y-axis, which makes movement in the x-direction transverse movement. When considering a structure of multiple beams, it is important that the same global coordinate system is used for all of the beams in the structure, since only one global stiffness and mass matrix will be used. For the model in this research project, a coordinate system is chosen where the ground is parallel to the x-axis and the building is parallel to the y-axis. This leads to the requirement that the displacement of all of the beams should be transformed such that these align with the described global coordinate system.

The beam elements of the building are not parallel to the y-axis, except for the wall elements. Since transverse beam displacement will be in the x-direction and axial beam displacement will be in the y-direction, these wall elements are already oriented correctly. This means that the floor elements and the diagonal elements in both directions should be transformed to match the global coordinate system. Combining the transverse and axial motion matrices and transforming part of the beam elements of the model is discussed in sections II-D2 and II-D3 respectively.

2) Combining transverse and axial motion
The deflection of a beam is determined by calculating the displacement of the two nodes which are located at the ends of a beam element, by using the local stiffness and mass matrices, in which the behaviour of the beams is captured. One stiffness and mass matrix contain values for all of the degrees of freedom of one beam element. Since each beam has two nodes and each node has 3 degrees of freedom, a total of 6 degrees of freedom have to be represented by the stiffness and mass matrix, which means that these matrices will be 6×6 matrices, where every row and column represents a

single degree of freedom. The displacement vector of these nodes will be represented as

$$\mathbf{u} = \begin{bmatrix} u_1 \\ u_2 \\ u_3 \\ u_4 \\ u_5 \\ u_6 \end{bmatrix}, \tag{20}$$

where the values u_1, u_2 and u_3 will represent the displacements in the directions as explained below Eq. (18) for node 1 of the beam element and the values u_4, u_5 and u_6 will represent the displacements in the directions as explained below Eq. (18) for node 2 of the beam element.

Now, Eqs. (8) and (16) can be combined such that these correspond to the correct displacement values. Also, Eqs. (9) and (17) can be combined in the same way. This gives:

$$\mathbf{k} = \left(\frac{EI}{L^3}\right) \begin{bmatrix} 12 & 0 & 6L & -12 & 0 & 6L \\ 0 & \frac{AL^2}{I} & 0 & 0 & -\frac{AL^2}{I} & 0 \\ 6L & 0 & 4L^2 & -6L & 0 & 2L^2 \\ -12 & 0 & -6L & 12 & 0 & -6L \\ 0 & -\frac{AL^2}{I} & 0 & 0 & \frac{AL^2}{I} & 0 \\ 6L & 0 & 2L^2 & -6L & 0 & 4L^2 \end{bmatrix} \tag{21}$$

$$\mathbf{m} = \left(\frac{\rho AL}{420}\right) \begin{bmatrix} 156 & 0 & 22L & 54 & 0 & -13L \\ 0 & 140 & 0 & 0 & 70 & 0 \\ 22L & 0 & 4L^2 & 13L & 0 & -3L^2 \\ 54 & 0 & 13L & 156 & 0 & -22L \\ 0 & 70 & 0 & 0 & 140 & 0 \\ -13L & 0 & -3L^2 & -22L & 0 & 4L^2 \end{bmatrix} \tag{22}$$

These matrices are the local stiffness and mass matrices respectively, which are used in the model to construct the global stiffness and mass matrix. The construction of the global stiffness and mass matrix is discussed in section II-D4.

3) Transformation of beam elements
The local stiffness and mass matrices shown in Eqs. (21) and (22) respectively are valid for beam elements which are oriented parallel to the y-axis in the global coordinate system. Therefore, for all of the elements that are not parallel to the y-axis, i.e. the floor elements and the diagonal elements in both directions, the stiffness and mass matrices should be transformed such that the element properties align with the global coordinate system. This can be done by using a transformation matrix. Let u be the displacements in the local coordinate system and let $\hat{u}$ be the displacements in the global coordinate system. Then the relations between these displacements are

$$u_1 = \hat{u_1}\cos(\theta) + \hat{u_2}\sin(\theta), \tag{23}$$

$$u_2 = -\hat{u_1}\sin(\theta) + \hat{u_2}\cos(\theta), \tag{24}$$

and

$$u_3 = \hat{u_3}, \tag{25}$$

for the first node of the beam element. For the second node, the relations are the same, but here u_4, u_5, u_6, $\hat{u_4}$, $\hat{u_5}$ and $\hat{u_6}$ are used instead of u_1, u_2, u_3, $\hat{u_1}$, $\hat{u_2}$ and $\hat{u_3}$ respectively. The resulting 6 equations can be written in matrix notation, in the form of

$$\mathbf{u} = \mathbf{T}\hat{\mathbf{u}}, \tag{26}$$

where

$$\mathbf{u} = \begin{bmatrix} u_1 \\ u_2 \\ u_3 \\ u_4 \\ u_5 \\ u_6 \end{bmatrix}, \qquad \hat{\mathbf{u}} = \begin{bmatrix} \hat{u_1} \\ \hat{u_2} \\ \hat{u_3} \\ \hat{u_4} \\ \hat{u_5} \\ \hat{u_6} \end{bmatrix}. \tag{27}$$

This gives the following relation:

$$\begin{bmatrix} u_1 \\ u_2 \\ u_3 \\ u_4 \\ u_5 \\ u_6 \end{bmatrix} = \begin{bmatrix} \cos\theta & \sin\theta & 0 & 0 & 0 & 0 \\ -\sin\theta & \cos\theta & 0 & 0 & 0 & 0 \\ 0 & 0 & 1 & 0 & 0 & 0 \\ 0 & 0 & 0 & \cos\theta & \sin\theta & 0 \\ 0 & 0 & 0 & -\sin\theta & \cos\theta & 0 \\ 0 & 0 & 0 & 0 & 0 & 1 \end{bmatrix} \begin{bmatrix} \hat{u_1} \\ \hat{u_2} \\ \hat{u_3} \\ \hat{u_4} \\ \hat{u_5} \\ \hat{u_6} \end{bmatrix} \tag{28}$$

Which means that the transformation matrix for a beam element (containing 2 nodes) is found to be equal to:

$$\mathbf{T} = \begin{bmatrix} \cos\theta & \sin\theta & 0 & 0 & 0 & 0 \\ -\sin\theta & \cos\theta & 0 & 0 & 0 & 0 \\ 0 & 0 & 1 & 0 & 0 & 0 \\ 0 & 0 & 0 & \cos\theta & \sin\theta & 0 \\ 0 & 0 & 0 & -\sin\theta & \cos\theta & 0 \\ 0 & 0 & 0 & 0 & 0 & 1 \end{bmatrix} \tag{29}$$

where θ is the angle with which the beam element should be rotated to align with the global coordinate system.

This transformation matrix can now be used to transform the local stiffness and mass matrices of the floor and diagonal elements by using the equations

$$\hat{\mathbf{k}} = \mathbf{T}^T\mathbf{k}\mathbf{T} \tag{30}$$

and

$$\hat{\mathbf{m}} = \mathbf{T}^T\mathbf{m}\mathbf{T} \tag{31}$$

respectively. For the derivation of Eqs. (30) and (31) see 'Structural Dynamics'[32] (pp. 397-399). Now, the stiffness and mass matrices of the floor elements and diagonal elements can be transformed, by filling in Eq. (29) in combination with the local stiffness matrix $\mathbf{k}$ and the local mass matrix $\mathbf{m}$ in Eqs. (30) and (31) respectively.

Forces on the building are applied in the global coordinate system, which means that the force vector does not have to be transformed.

4) Global stiffness and mass matrices
Using the transformed local stiffness and mass matrices, global stiffness and mass matrices can be constructed, which describe the entire structure. The local stiffness and mass matrices describe the behaviour of single beams in the structure, with

which two nodes are connected. Although the same material properties are used for all of the beams of the structure, not all of the beams have the same length. Also, the beam elements have to be transformed using different angles, depending on where in the structure the beam elements are located. In order to create global stiffness and mass matrices using the constructed local stiffness and mass matrices, an $n \times n$ matrix should be constructed, where n is the amount of degrees of freedom of the structure. Therefore, the row and column numbers correspond to the separate degrees of freedom. Now, the local stiffness and mass matrices can be used as sub-matrices, where connections can be made between degrees of freedom by filling in the corresponding values from these local matrices. For example, if the first and second node of the structure are connected by a beam element, the local stiffness and mass matrices as shown in Eqs. (21) and (22) can be filled in to the corresponding locations of the first and second node in the global stiffness and mass matrices respectively, which are the locations in the 6×6 sub-matrix in the top left corner of both global matrices. When two nodes are connected that are not adjacent values, the local stiffness and mass matrices can be divided into four equally sized 3×3 sub-matrices, as

$$\hat{\mathbf{k}} = \begin{bmatrix} \hat{\mathbf{k}}_{11} & \hat{\mathbf{k}}_{12} \\ \hat{\mathbf{k}}_{21} & \hat{\mathbf{k}}_{22} \end{bmatrix} \quad (32)$$

and

$$\hat{\mathbf{m}} = \begin{bmatrix} \hat{\mathbf{m}}_{11} & \hat{\mathbf{m}}_{12} \\ \hat{\mathbf{m}}_{21} & \hat{\mathbf{m}}_{22} \end{bmatrix}, \quad (33)$$

where the general sub-matrix form can be denoted as k_{ij} and m_{ij} and the subscript values correspond to the node that is represented in the row and in the column for i and j respectively. The values from the stiffness and mass matrices that correspond to the combination of nodes of the subscript are represented by that sub-matrix. Now, each sub-matrix can be inserted into the global matrices, to the location where the combination of nodes corresponds to the same combination of nodes in the global matrices. This gives global stiffness and mass matrices in the following form:

$$\mathbf{K} = \begin{bmatrix} \hat{\mathbf{k}}_{11} & \hat{\mathbf{k}}_{12} & \cdots & \cdots & \cdots & \cdots & \hat{\mathbf{k}}_{1n} \\ \hat{\mathbf{k}}_{21} & \hat{\mathbf{k}}_{22} & \cdots & \cdots & \cdots & \cdots & \hat{\mathbf{k}}_{2n} \\ \vdots & \vdots & \ddots & & & & \vdots \\ \vdots & \vdots & & \hat{\mathbf{k}}_{xx} & \hat{\mathbf{k}}_{xy} & & \vdots \\ \vdots & \vdots & & \hat{\mathbf{k}}_{yx} & \hat{\mathbf{k}}_{yy} & & \vdots \\ \vdots & \vdots & & & & \ddots & \vdots \\ \hat{\mathbf{k}}_{n1} & \hat{\mathbf{k}}_{n2} & \cdots & \cdots & \cdots & \cdots & \hat{\mathbf{k}}_{nn} \end{bmatrix} \quad (34)$$

$$\mathbf{M} = \begin{bmatrix} \hat{\mathbf{m}}_{11} & \hat{\mathbf{m}}_{12} & \cdots & \cdots & \cdots & \cdots & \hat{\mathbf{m}}_{1n} \\ \hat{\mathbf{m}}_{21} & \hat{\mathbf{m}}_{22} & \cdots & \cdots & \cdots & \cdots & \hat{\mathbf{m}}_{2n} \\ \vdots & \vdots & \ddots & & & & \vdots \\ \vdots & \vdots & & \hat{\mathbf{m}}_{xx} & \hat{\mathbf{m}}_{xy} & & \vdots \\ \vdots & \vdots & & \hat{\mathbf{m}}_{yx} & \hat{\mathbf{m}}_{yy} & & \vdots \\ \vdots & \vdots & & & & \ddots & \vdots \\ \hat{\mathbf{m}}_{n1} & \hat{\mathbf{m}}_{n2} & \cdots & \cdots & \cdots & \cdots & \hat{\mathbf{m}}_{nn} \end{bmatrix} \quad (35)$$

These global matrices will be used in the calculation of the dynamic behaviour of the building in the building model.

E. Beam properties

The dynamic behaviour of the building model is highly dependent on the properties of the beams with which the building is constructed. This can also be seen from the local stiffness and mass matrices in Eqs. (21) and (22), where the elasticity modulus E, the moment of inertia I, the length L, the cross-sectional area A and the density ρ of the beam elements are taken into account. The chosen material for the beams of the building model is steel, since most of the building is constructed from steel[33] and concrete. This gives the required elasticity modulus and density of the material, shown in Table II. In order to determine the moment of inertia and the cross sectional area of the beams, a beam shape should be chosen. An I-beam was chosen, since this is a simple shape from which the moment of inertia can easily be tuned to the correct value. This tweaking of the moment of inertia is necessary in order to make the natural oscillation frequency and the mass of the building model equal to the natural oscillation frequency and the mass of the actual building. The first and fundamental mode is the most important mode that must be matched accurately, since this mode describes the main oscillation frequency of the building, which determines the main dynamic behaviour. Matching the natural oscillation frequency of the building was done by iteratively changing the I-beam dimensions and comparing the eigenfrequencies of the building model and the actual building by doing an eigenvalue study, which is explained further in section II-F. The correct mass of the building is determined by taking into account that the mass of the TMD system in the actual building is equal to 0.24%[33] of the total building mass. The I-beam dimensions were tweaked until the building mass resulted in the correct pendulum mass of $660000kg$ and the frequency was tuned as close as possible to the natural oscillation frequency of the actual building. The moment of inertia[34] of an I-beam around the horizontal axis (the axis parallel to the flanges of the I-beam, located in the middle between the flanges of the I-beam) is given by

$$I_x = \frac{wh^3}{12} - \frac{(w - t_w)(h - 2t_f)^3}{12} \quad (36)$$

where w is the width of the flange, h is the height of the I-beam, t_f is the thickness of the flange and t_w is the thickness of the web. These variables are clarified in Figure 2. The I-beam dimensions that where found to most accurately match the natural oscillation frequency of the building, are shown in Table I.

	w	h	t_f	t_w
Dimension (m)	3.34	3.34	0.50	0.50

TABLE I: Dimensions of the I-beams of the building model.

All of the beams of the structure are chosen to be almost the same. However, the length of the different beam elements can differ based on the part of the building that is represented by the beam element. The length of the beam elements is
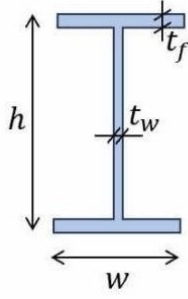
Fig. 2: I-beam configuration.

determined based on the dimensions of the Taipei 101 building in combination with the simplification of the model, where a rectangular structure is used. The properties of the steel beams of the structure are shown in Table II, where the distinction is made between floor, diagonal and wall elements. The length of the different elements is represented visually in the building model shown in Figure 24.

	Floor	Diagonal	Wall
Elasticity modulus (GPa)	200	200	200
Density (kg/m^3)	7850	7850	7850
Moment of inertia $(kg \cdot m^2)$	7.3382	7.3382	7.3382
Cross-sectional area (m^2)	4.510	4.510	4.510
Length (m)	45	45.883	8.960

TABLE II: Properties[33][35][36] of the different beam elements in the building model.

F. Internal building damping

In order to model the internal damping of the material of the building, Rayleigh damping will be used. Rayleigh damping[32] is a form of damping that is often used for modelling structures. It uses proportional damping, where the damping matrix is constructed by multiplying the global mass and stiffness matrix of the system by two constants, in the form of

$$\mathbf{C} = \alpha\mathbf{M} + \beta\mathbf{K}, \tag{37}$$

where the constants α and β can be chosen based on the required damping properties of the building. The mass and stiffness proportional damping contribute to damping the lower and higher frequencies of the building dynamics respectively. This means that the values of α and β can be chosen such that the correct frequencies are damped out in a way that approximates the dynamic behaviour of the actual building most appropriately. The damping ratio for the nth vibration mode is

$$\zeta_n = \frac{1}{2}\left(\frac{\alpha}{\omega_n} + \beta\omega_n\right), \tag{38}$$

where ω_n is the natural frequency of the nth vibration mode. For convenience, the angular natural frequency ω_n is transformed to the natural frequency f_n, using $\omega_n = 2\pi \cdot f_n$, which gives

$$\zeta_n = \frac{1}{2}\left(\frac{\alpha}{2\pi \cdot f_n} + \beta \cdot 2\pi \cdot f_n\right). \tag{39}$$

When the damping ratios and natural frequencies of two modes are known, two equations can be obtained, one for each mode, which allows to solve for the two remaining unknowns, α and β. When building a new structure, a damping ratio can be chosen based on the maximum allowed structural displacement, such that discomfort for building residents and damage to the structure is prevented. However, in this case, the damping ratio of the different modes of the Taipei 101 building should be approximated. The first three modes of the building are taken into account for this. Based on measurement results[29] from the 'Masta', 'Talim' and 'Krosa' typhoons and the 'Wenchuan' earthquake, the average damping ratios and natural frequencies for the first three modes of vibration are shown in Table III.

	Mode 1	Mode 2	Mode 3
Damping ratio (%)	1.65	1.21	0.76
Natural frequency (Hz)	0.149	0.429	0.779

TABLE III: Average damping ratios and natural frequencies of the Taipei 101 building, measured[29] from various typhoons and an earthquake.

The damping ratios for the different modes of vibration in the model can be approximated by using the measured values in Table III. The natural frequencies of the different modes of vibration in the model should be determined based on the structure in the model itself. The natural frequencies of the building model are determined using an eigenvalue study, where the eigenvectors and eigenfrequencies of the building are determined based on the global stiffness and mass matrices of the building.

The obtained eigenvectors represent the mode shapes (building deflection shapes) of the different modes and the eigenfrequencies represent the natural frequencies of the modes. As explained in section II-E, the structure of the building model was changed such that the most significant modes, which are the lowest modes, match the measured natural frequencies shown in Table III as closely as possible. The final modes of vibration of the building model are equal to $0.1043Hz$, $0.5756Hz$ and $0.9548Hz$, for which the first mode had the highest priority to be matched as closely as possible, since this mode represents the main building oscillation.

Now, the values for α and β can be determined, using the first and second mode of the building and filling in the found values in Eq. (39), which gives

$$0.0165 = \frac{1}{2}\left(\frac{\alpha}{2\pi \cdot 0.1043} + \beta \cdot 2\pi \cdot 0.1043\right) \tag{40}$$

and

$$0.0121 = \frac{1}{2}\left(\frac{\alpha}{2\pi \cdot 0.5756} + \beta \cdot 2\pi \cdot 0.5756\right), \tag{41}$$

where solving for α and β gives values of $\alpha = 0.01939$ and $\beta = 0.005209$. These values can be filled in in Eq. (37), which gives

$$\mathbf{C} = 0.01939 \cdot \mathbf{M} + 0.005209 \cdot \mathbf{K}, \tag{42}$$

which provides the damping matrix for the building model. Now, when plotting the damping ratio against the natural frequencies of the different vibration modes using Eq. (39) and the values of $\alpha = 0.01939$ and $\beta = 0.005209$, a damping plot is obtained which is shown in Figure 3.
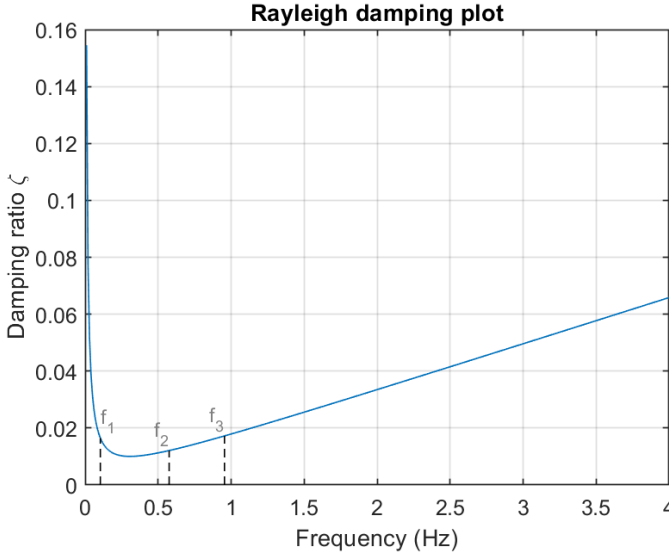

Fig. 3: Rayleigh damping plot using $\alpha = 0.01939$ and $\beta = 0.005209$.

Although the calculated values of α and β are theoretically correct, in the model used in this research project, numerical instability occurs when using these values. It was found that this numerical instability was caused by the value of β. Therefore, the numerical instability is most likely caused by overdamping, due to the high stiffness of the building. Because of this, a slightly lower value of $\beta = 0.0001$ was chosen, which does not induce numerical instability but does damp out the higher frequency oscillations of the building, leading to a smoother simulation. The corresponding value of α was determined using equation 39, using only the fundamental frequency of $f_n = 0.1043 Hz$ and the corresponding damping ratio of $\zeta = 0.0165$. This leads to new values of $\alpha = 0.02120$ and $\beta = 0.0001$. See section V-D for more explanation about these values in combination with the simulations. The corresponding Rayleigh damping plot is shown in Figure 4. It can be seen that the damping on the fundamental eigenfrequency f_1 is barely affected by the change in Rayleigh damping parameters. The second and third eigenfrequencies are damped less than in the theoretically correct case of Figure 3.

G. Building equations of motion

The equations of motion of the building can be constructed, using the found global mass, stiffness and damping matrices. The equation of motion of the building is

$$\mathbf{M\ddot{u}} + \mathbf{C\dot{u}} + \mathbf{Ku} = \mathbf{F}, \tag{43}$$

where $\mathbf{M}$ is the global mass matrix, $\mathbf{C}$ is the global damping matrix, $\mathbf{K}$ is the global stiffness matrix, $\mathbf{F}$ is the force vector, which represents forces to the building nodes and $\mathbf{\ddot{u}}$, $\mathbf{\dot{u}}$ and
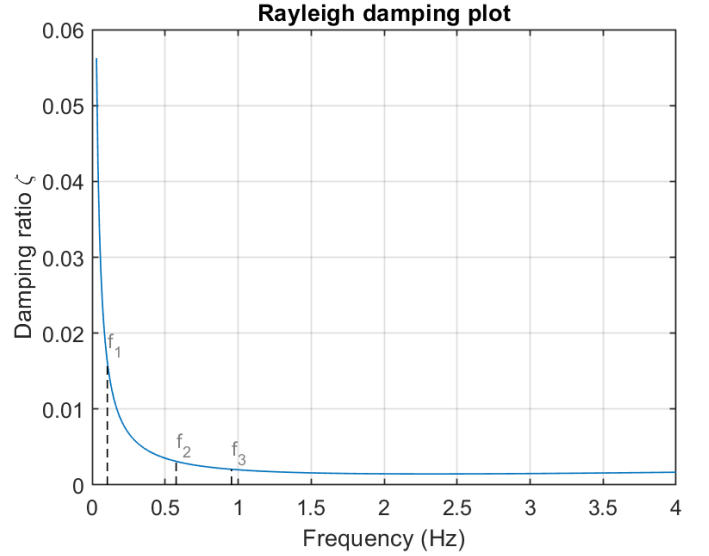

Fig. 4: Rayleigh damping plot using $\alpha = 0.02120$ and $\beta = 0.0001$.

$\mathbf{u}$ are the acceleration vector, velocity vector and position vector of the building nodes respectively. The global mass, damping and stiffness matrices consist of values that represent connections between degrees of freedom of the nodes of the building, as explained in section II-D4. The pendulum TMD system in the building model consists of a mass which is attached to the building with a cable. The location where this cable is attached to the building will be called the 'pendulum connection point' or 'pendulum attachment point'. In the building model, this pendulum connection point is represented by a node, which is part of the building structure. This node will be called the 'connection node', while the rest of the nodes will be called 'free nodes'. All of the building nodes in the matrices are located in the order of the building nodes, as depicted by the node numbers shown in Figure 24, which means that the degrees of freedom corresponding to the connection node are located somewhere in the middle of the matrix. In order to simplify the theoretical analysis, the global mass, damping and stiffness matrices are reordered, such that the sub-matrix corresponding to the degrees of freedom of the connection node is located at the bottom right of all of the global matrices. Also, the acceleration, velocity, position and force vectors are reordered such that the sub-vector that corresponds to the degrees of freedom of the connection node is located at the bottom of all of the vectors. This can be depicted by

$$\mathbf{M} = \begin{bmatrix} \mathbf{M}_{ff} & \mathbf{M}_{fc} \\ \mathbf{M}_{cf} & \mathbf{M}_{cc} \end{bmatrix}, \quad \mathbf{K} = \begin{bmatrix} \mathbf{K}_{ff} & \mathbf{K}_{fc} \\ \mathbf{K}_{cf} & \mathbf{K}_{cc} \end{bmatrix}, \quad \mathbf{C} = \begin{bmatrix} \mathbf{C}_{ff} & \mathbf{C}_{fc} \\ \mathbf{C}_{cf} & \mathbf{C}_{cc} \end{bmatrix} \tag{44}$$

and

$$\mathbf{\ddot{u}} = \begin{bmatrix} \mathbf{\ddot{u}}_f \\ \mathbf{\ddot{u}}_c \end{bmatrix}, \quad \mathbf{\dot{u}} = \begin{bmatrix} \mathbf{\dot{u}}_f \\ \mathbf{\dot{u}}_c \end{bmatrix}, \quad \mathbf{u} = \begin{bmatrix} \mathbf{u}_f \\ \mathbf{u}_c \end{bmatrix}, \quad \mathbf{F} = \begin{bmatrix} \mathbf{F}_f \\ \mathbf{F}_c \end{bmatrix}, \tag{45}$$

where the subscript f represents the free nodes and the subscript c represents the connection node. This means that for the subscript ff, all connections are meant between the

degrees of freedom of two free nodes. The subscript fc and cf resemble the connections between the degrees of freedom of one free node and the connection node and the subscript cc resembles the connections between the degrees of freedom of the connection node itself. Filling in the matrices and vectors of Eqs. (44) and (45) into Eq. (43) gives

$$\begin{bmatrix} \mathbf{M}_{ff} & \mathbf{M}_{fc} \\ \mathbf{M}_{cf} & \mathbf{M}_{cc} \end{bmatrix} \begin{bmatrix} \ddot{\mathbf{u}}_f \\ \ddot{\mathbf{u}}_c \end{bmatrix} + \begin{bmatrix} \mathbf{C}_{ff} & \mathbf{C}_{fc} \\ \mathbf{C}_{cf} & \mathbf{C}_{cc} \end{bmatrix} \begin{bmatrix} \dot{\mathbf{u}}_f \\ \dot{\mathbf{u}}_c \end{bmatrix} + \\ \begin{bmatrix} \mathbf{K}_{ff} & \mathbf{K}_{fc} \\ \mathbf{K}_{cf} & \mathbf{K}_{cc} \end{bmatrix} \begin{bmatrix} \mathbf{u}_f \\ \mathbf{u}_c \end{bmatrix} = \begin{bmatrix} \mathbf{F}_f \\ \mathbf{F}_c \end{bmatrix}, \quad (46)$$

which are the building equations of motion.

H. Pendulum tuned mass damper system

The Taipei 101 building is equipped with a $660000kg$[37] pendulum tuned mass damper (TMD) system, which is used to suppress vibrations due to external forces that are applied to the building due to wind gusts or seismic activity. In Figure 5, a schematic of this TMD system is shown. The pendulum is hanging on 92 steel cables, which are all $42m$ in length. Furthermore, the pendulum is damped using 8 hydraulic dampers, which are attached to the pendulum mass itself and are able to rotate along with the pendulum at the location where these dampers are attached to the building structure. Also, below the pendulum mass, a ring is attached which is damped by 8 more hydraulic dampers, which is done to further reduce the movement of the pendulum TMD to a maximum of around $1.50m$.
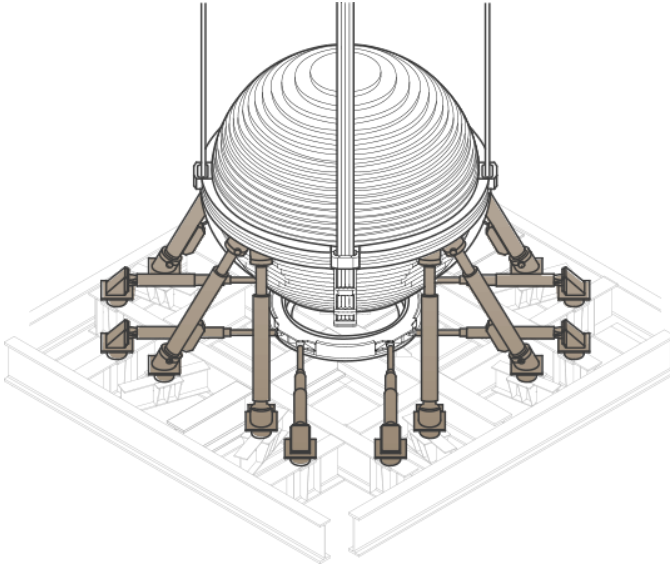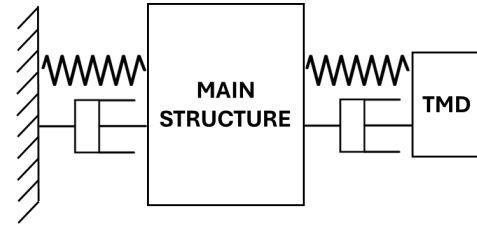

Fig. 5: Taipei 101 pendulum TMD system[37].

In this section, a (pendulum) TMD system is explained and the pendulum equations of motion are derived. Also, the natural frequency and damping of the pendulum are discussed and the coupling of the pendulum to the building is described.

1) Tuned mass damper system

Tuned mass dampers systems can been used to suppress the vibration of structures. Wind gusts or seismic activity can cause a large structure to vibrate, which can cause damage to the structure or lead to discomfort for building occupants. Wind gusts and seismic activity mainly cause problems when the forces occur in a frequency that is around the natural oscillation frequency of the fundamental mode of the structure, because the external forces could cause resonance in the oscillation of the structure, which can lead to oscillations that are higher in amplitude. In order to mitigate this resonance, another external force is added to the main structure, in the form of a TMD system. Using this system, vibration mitigation is achieved by tuning the mass damper system such that it opposes the movement of the main structure to which it is attached. Tuning of the TMD system is performed by changing the properties of the spring and damper with which the TMD system is attached to the main structure, such that the natural frequency of the TMD system oscillation is the same as the natural frequency of the fundamental mode of oscillation of the main structure. This created antiresonance between the oscillations of the pendulum and the main structure, which causes the kinetic energy of the oscillation of the structure to be transferred to the TMD mass and dissipated using dampers. Although the mass of a TMD system is typically much smaller than the mass of the main structure (0.24%[33] of the building mass in the case of the Taipei 101 pendulum TMD), it is still able to reduce the vibration of the main structure, due to this antiresonance. A schematic of a simple linear TMD system is shown in Figure 6a.

(a) Linear TMD system
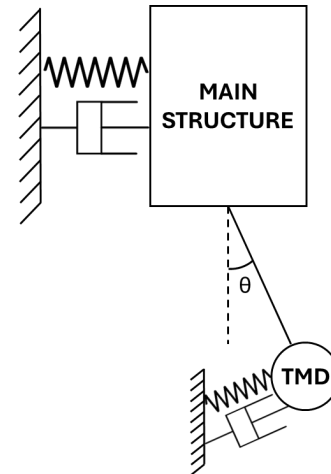
(b) Pendulum TMD system

Fig. 6: Two types of TMD systems.

The Taipei 101 building does not use a linear TMD system, but a pendulum TMD system. A pendulum TMD system

works in the same way as the linear variant, since this system is also tuned such that the natural oscillation frequency matches the natural oscillation frequency of the building to create antiresonance for vibration mitigation. In Figure 6b, a schematic is shown of a simple pendulum TMD system. While a linear TMD is connected to the main structure directly using springs and dampers, a pendulum TMD is hanging on the structure using cables, while also being attached to the building using dampers, which are usually connected to the pendulum mass as shown in Figure 5. Also, springs can be added to modify the natural frequency of the pendulum TMD. When the structure starts to displace due to external forces, the angle of the pendulum cable with the vertical increases, which causes the pendulum mass experiences a restoring torque due to gravity, which is pointed towards the equilibrium point. This causes a force on the connection point of the pendulum, which is in the opposite direction and thus, the connection point is 'pulled' back to the equilibrium position by the pendulum, which creates the antiresonance.

2) Pendulum equations of motion
The equations of motion of the pendulum can be constructed, using the equation of motion of a simple pendulum, where only the angle θ between the pendulum cable and the vertical is needed to describe the pendulum motion. However, for the pendulum TMD in the building model, the connection point of the pendulum is not fixed, since the connection node is part of the building structure, which can move due to external forces. Therefore, the movement of the connection node has to be taken into account as well when deriving the equations of motion of the pendulum. First, the sum of moments around the connection point of the pendulum should be taken as

$$\sum M_z = I\alpha, \tag{47}$$

where I is the moment of inertia of the pendulum and α is the angular acceleration of the pendulum. The moment of inertia of the pendulum is equal to

$$I = mL^2, \tag{48}$$

where m is the mass of the pendulum bob and L is the length from the connection point to the pendulum mass. Also, since the angle θ will be used to describe the system, the angular acceleration of the pendulum is equal to the second derivative of the angle, which gives $\alpha = \ddot{\theta}$. Also, the sum of moments around the connection point of the pendulum is equal to the pendulum torque, so $\sum M_z = \tau_z$. Filling in all of the found variables in Eq. (47) gives

$$\tau_z = mL^2\ddot{\theta}. \tag{49}$$

The torque of the pendulum can be calculated using

$$\boldsymbol{\tau} = \mathbf{r} \times \mathbf{F}, \tag{50}$$

where $\boldsymbol{\tau}$ is the torque vector, $\mathbf{F}$ is the force vector and $\mathbf{r}$ is the position vector, which in turn consists of two vectors

$$\mathbf{r} = \mathbf{r}_{pivot} + \mathbf{r}_{pend}, \tag{51}$$

where $\mathbf{r}_{pivot}$ points from the origin to the pivot point (connection point) of the pendulum and $\mathbf{r}_{pend}$ points from the pivot point to the mass of the pendulum. When the origin is taken to move along with the location of the pivot point, $\mathbf{r}_{pivot} = \mathbf{0}$, so the position vector becomes

$$\mathbf{r} = \mathbf{r}_{pend} = \begin{bmatrix} L\sin(\theta) \\ L\cos(\theta) \\ 0 \end{bmatrix}, \tag{52}$$

where the displacement in the z-direction is equal to zero in this 2D scenario. The force vector is

$$\mathbf{F} = \begin{bmatrix} m\ddot{u}_x \\ m\ddot{u}_y - mg \\ 0 \end{bmatrix}, \tag{53}$$

where the acceleration of the connection point in the x- and y-direction are taken into account, as well as the gravitational force acting in the y-direction. By substituting the found position and force vectors into Eq. (50), the torque vector becomes

$$\boldsymbol{\tau} = \begin{bmatrix} 0 \\ 0 \\ L\sin(\theta) \cdot (m\ddot{u}_y - mg) - L\cos(\theta) \cdot m\ddot{u}_x \end{bmatrix}, \tag{54}$$

which means that the torque in the z-direction (which also is the magnitude of the torque in this case) is equal to

$$\tau_z = L\sin(\theta) \cdot (m\ddot{u}_y - mg) - L\cos(\theta) \cdot m\ddot{u}_x, \tag{55}$$

which can be filled in into Eq. (49), which gives

$$mL^2\ddot{\theta} = L\sin(\theta) \cdot (m\ddot{u}_y - mg) - L\cos(\theta) \cdot m\ddot{u}_x, \tag{56}$$

which is the equation of motion of the pendulum system with moving connection point, without any springs or dampers.

3) Pendulum natural frequency and damping
As discussed in section II-H1, the natural oscillation frequency of the pendulum should be tuned such that it is equal to the natural frequency of the fundamental oscillation mode of the building, such that antiresonance can be achieved to mitigate the building oscillation. For small angles θ, i.e. $\theta \ll 1rad$, the natural oscillation frequency of a simple pendulum is given by

$$f = \frac{1}{2\pi}\sqrt{\frac{g}{L}}, \tag{57}$$

where g is the gravitational constant and L is the pendulum length. In the actual building, the dampers are implemented at the bottom of the system and attached to the pendulum bob. However, in order to be able to modify the natural frequency of the pendulum TMD in the model to approximate the behaviour of the TMD system in the Taipei 101 building, rotational springs and dampers will be implemented in the model. The springs contribute to the natural frequency of the pendulum. The natural frequency including the effect of the rotational springs is given by

$$f = \frac{1}{2\pi}\sqrt{\frac{k + mgL}{I}} = \frac{1}{2\pi}\sqrt{\frac{k + mgL}{mL^2}}, \tag{58}$$

where k is the spring constant. The natural frequency of the fundamental mode of the building model was found to be $0.1043 Hz$ (refer to section II-F). Furthermore, the length of the pendulum cables in the Taipei 101 building are equal to $42m$[37]. The mass of the pendulum bob in the building model is set to 0.24% of the mass of the entire building in the model, as discussed before. In the model, the mass of the pendulum bob is $660998kg$. Filling in these values for the variables f, L and m respectively in Eq. (58) and solving for k gives a rotational pendulum spring constant of $k = 228412534 Nm/rad$.

Now, also the rotational pendulum damping can be determined. The damping coefficient b can be determined using

$$b = 2\zeta_p \sqrt{Ik} = 2\zeta_p \sqrt{mL^2 k}, \tag{59}$$

where ζ_p is the pendulum damping ratio and k is the rotational pendulum spring constant. In order to determine the damping coefficient b, the damping ratio ζ_p should be determined, which can be done based on the maximum allowed pendulum deflection during a strong hurricane. The pendulum system in the Taipei 101 building has a maximum swing of $1.50m$[37] during such high wind forces. This means that the pendulum bob can swing $1.50m$ in all directions away from the equilibrium position. A strong hurricane was defined as having a wind velocity of $32.78m/s$[38] at a height of $10m$. Using the finished model, a value of $\zeta_p = 0.30$ was found to provide this maximum swing of $1.50m$ at the wind velocity of $32.78m/s$ at a height of $10m$. In Figure 13, this maximum swing is shown. Using a damping ratio of $\zeta_p = 0.30$ and filling in Eq. (59), the damping coefficient becomes $b = 309642423 Nm \cdot s/rad$.

In order to implement the found spring constant and damping coefficient to the pendulum model, the variables can be added to the equation of motion. The spring constant is proportional to the pendulum deflection angle θ and the damping coefficient is proportional to the pendulum angular velocity $\dot{\theta}$. The rotational spring causes a restoring force, which causes the torque due to the spring to be in the negative direction for positive angles of θ and in the positive direction for negative angles of θ. The rotational damper causes a damping torque, which works against the direction of motion such that the torque due to the damper is negative if the angular velocity $\dot{\theta}$ is positive and positive if the angular velocity $\dot{\theta}$ is negative. Therefore, the pendulum equation of motion becomes

$$mL^2\ddot{\theta} = (u_x + L\sin(\theta)) \cdot (m\ddot{u}_y - mg) - (u_y - L\cos(\theta)) \cdot (m\ddot{u}_x) - b\dot{\theta} - k\theta, \tag{60}$$

which is the final equation of motion of the pendulum system with moving connection point, including springs and dampers. The spring constant and damping coefficient will be implemented in the final equations of motion of the building, which will be explained in section II-H4.

4) Pendulum coupling to the building
When the building moves due to wind forces or seismic activity, it exerts a certain force on the pendulum bob, due to the displacement of the connection point, as discussed in section II-H2. In the real pendulum system, the force on the connection point causes a tension in the pendulum cables, which acts on the pendulum and thus pulls the pendulum towards the new location. This force on the connection point also causes a torque on the pendulum bob, which is implemented in the pendulum equation of motion (Eq. (60)). Additionally, the pendulum angle θ changes which gives a restoring torque due to gravity. In the building model, the torques on the pendulum, which are described above, are applied to the pendulum bob, but the tension force from the pendulum cables, which is caused by the force on the connection point, is not applied to the pendulum bob. Instead, the pendulum bob is displaced by the same amount as the connection point, after which the angle θ of the pendulum is determined due to the mentioned torques, which correctly describes the pendulum motion.

However, in order for the TMD system to work appropriately, the pendulum bob should apply a force to the connection node as well, which causes the building to be 'pulled' back by the pendulum due to antiresonance. By Newton's third law, it is known that the force that is exerted on the pendulum, also exerts an equal and opposite force on the connection node of the building. This force on the connection node is applied through the tension in the pendulum cable, in which the forces from the torque are taken into account, in addition to the force due to the displacement of the pendulum bob (which is caused by the displacement of the connection point) and the force due to gravity on the pendulum bob. In order to determine the forces in x- and y-direction on the connection node, due to the pendulum, the force acting on the pendulum in the x- and y-direction should be determined, which can be done by starting with the displacement of the pendulum in x- and y-direction, which is

$$x = u_x + L\sin(\theta) \tag{61}$$

and

$$y = u_y + L - L\cos(\theta). \tag{62}$$

Now, the derivative and second derivative of these displacements can be taken, which gives

$$\dot{x} = \dot{u}_x + \dot{\theta}L\cos(\theta), \tag{63}$$

$$\dot{y} = \dot{u}_y + \dot{\theta}L\sin(\theta) \tag{64}$$

and

$$\ddot{x} = \ddot{u}_x + \ddot{\theta}L\cos(\theta) - \dot{\theta}^2 L\sin(\theta), \tag{65}$$

$$\ddot{y} = \ddot{u}_y + \ddot{\theta}L\sin(\theta) + \dot{\theta}^2 L\cos(\theta). \tag{66}$$

Now, the force on the pendulum bob in the x- and y-direction can be determined using Newton's second law, which gives

$$\sum F_x = \lambda_x = m\ddot{x}, \tag{67}$$

and

$$\sum F_y = \lambda_y - mg = m\ddot{y}, \tag{68}$$

where λ_x and λ_y are the forces that are applied on the pendulum due to forces on the connection point. Now, the pendulum acceleration in x- and y-direction from Eqs. (65) and (66) can be filled in in Eqs. (67) and (68) respectively, which gives

$$\lambda_x = m(\ddot{u}_x + \ddot{\theta}L\cos(\theta) - \dot{\theta}^2 L\sin(\theta)) \tag{69}$$

and

$$\lambda_y = mg + m(\ddot{u}_y + \ddot{\theta}L\sin(\theta) + \dot{\theta}^2 L\cos(\theta)). \tag{70}$$

Now, using these forces on the pendulum, the force on the connection point can be determined using Newton's third law, which is

$$\lambda_x = -f_x \tag{71}$$

and

$$\lambda_y = -f_y, \tag{72}$$

where f_x and f_y are the forces on the connection node in the x- and y-direction respectively. Now remember from the building equation of motion that the forces on the connection point are denoted in the vector $\mathbf{F}_c$, where

$$\mathbf{F}_c = \begin{bmatrix} f_x \\ f_y \end{bmatrix}. \tag{73}$$

So, when filling in Eqs. (69) and (70) into Eqs. (71) and (72) and then filling in the obtained equations into Eq. (73), the connection point force vector becomes

$$\mathbf{F}_c = - \begin{bmatrix} m(\ddot{u}_x + \ddot{\theta}L\cos(\theta) - \dot{\theta}^2 L\sin(\theta)) \\ mg + m(\ddot{u}_y + \ddot{\theta}L\sin(\theta) + \dot{\theta}^2 L\cos(\theta)) \end{bmatrix}, \tag{74}$$

which can be divided into multiple separate vectors, which gives

$$\mathbf{F}_c = -m \left(\begin{bmatrix} \ddot{u}_x \\ \ddot{u}_y \end{bmatrix} + \begin{bmatrix} 0 \\ g \end{bmatrix} + \begin{bmatrix} \ddot{\theta}L\cos(\theta) - \dot{\theta}^2 L\sin(\theta) \\ \ddot{\theta}L\sin(\theta) + \dot{\theta}^2 L\cos(\theta) \end{bmatrix} \right). \tag{75}$$

Now, the value of $\ddot{\theta}$ can be filled in by substituting the $\ddot{\theta}$ from Eq. (56), which gives

$$\mathbf{F}_c = -m \left(\begin{bmatrix} \ddot{u}_x \\ \ddot{u}_y \end{bmatrix} + \begin{bmatrix} 0 \\ g \end{bmatrix} + \mathbf{B} \right), \tag{76}$$

where

$$\mathbf{B} = \begin{bmatrix} \left(\frac{L\sin(\theta)\cdot(m\ddot{u}_y - mg)}{mL^2} - \frac{L\cos(\theta)\cdot m\ddot{u}_x}{mL^2} \right)L\cos(\theta) - \dot{\theta}^2 L\sin(\theta) \\ \left(\frac{L\sin(\theta)\cdot(m\ddot{u}_y - mg)}{mL^2} - \frac{L\cos(\theta)\cdot m\ddot{u}_x}{mL^2} \right)L\sin(\theta) + \dot{\theta}^2 L\cos(\theta) \end{bmatrix}. \tag{77}$$

Now, Eq. (76) can be rewritten to give

$$\mathbf{F}_c = -m\boldsymbol{I}_2\left(\ddot{\mathbf{u}}_c + \mathbf{g} + \mathbf{B}\right), \tag{78}$$

where $\boldsymbol{I}_2$ is the identity matrix of size 2.

In order to couple these forces on the pendulum connection node to the building, the force vector has to be filled in in the equations of motion of the building. First, Eq. (46) should be expanded, which gives the equations

$$\mathbf{M}_{ff}\ddot{\mathbf{u}}_f + \mathbf{M}_{fc}\ddot{\mathbf{u}}_c + \mathbf{C}_{ff}\dot{\mathbf{u}}_f + \mathbf{C}_{fc}\dot{\mathbf{u}}_c + \mathbf{K}_{ff}\mathbf{u}_f + \mathbf{K}_{fc}\mathbf{u}_c = \mathbf{F}_f \tag{79}$$

and

$$\mathbf{M}_{cf}\ddot{\mathbf{u}}_f + \mathbf{M}_{cc}\ddot{\mathbf{u}}_c + \mathbf{C}_{cf}\dot{\mathbf{u}}_f + \mathbf{C}_{cc}\dot{\mathbf{u}}_c + \mathbf{K}_{cf}\mathbf{u}_f + \mathbf{K}_{cc}\mathbf{u}_c = \mathbf{F}_c. \tag{80}$$

Now, Eq. (78) can be filled in into Eq. (80), which gives

$$\mathbf{M}_{cf}\ddot{\mathbf{u}}_f + \mathbf{M}_{cc}\ddot{\mathbf{u}}_c + \mathbf{C}_{cf}\dot{\mathbf{u}}_f + \mathbf{C}_{cc}\dot{\mathbf{u}}_c + \mathbf{K}_{cf}\mathbf{u}_f + \mathbf{K}_{cc}\mathbf{u}_c = -m\boldsymbol{I}_2\left(\ddot{\mathbf{u}}_c + \mathbf{g} + \mathbf{B}\right), \tag{81}$$

which becomes

$$\mathbf{M}_{cf}\ddot{\mathbf{u}}_f + (\mathbf{M}_{cc} + m\boldsymbol{I}_2)\ddot{\mathbf{u}}_c + \mathbf{C}_{cf}\dot{\mathbf{u}}_f + \mathbf{C}_{cc}\dot{\mathbf{u}}_c + \mathbf{K}_{cf}\mathbf{u}_f + \mathbf{K}_{cc}\mathbf{u}_c + m\boldsymbol{I}_2\mathbf{g} + m\boldsymbol{I}_2\mathbf{B} = 0, \tag{82}$$

where the $\mathbf{M}_{cc} + m\boldsymbol{I}_2$ term will be denoted as $\overline{\mathbf{M}}_{cc}$. Now, the building equation of motion can be updated, where the new equation of motion is equal to

$$\begin{bmatrix} \mathbf{M}_{ff} & \mathbf{M}_{fc} \\ \mathbf{M}_{cf} & \overline{\mathbf{M}}_{cc} \end{bmatrix} \begin{bmatrix} \ddot{\mathbf{u}}_f \\ \ddot{\mathbf{u}}_c \end{bmatrix} + \begin{bmatrix} \mathbf{C}_{ff} & \mathbf{C}_{fc} \\ \mathbf{C}_{cf} & \mathbf{C}_{cc} \end{bmatrix} \begin{bmatrix} \dot{\mathbf{u}}_f \\ \dot{\mathbf{u}}_c \end{bmatrix} + \begin{bmatrix} \mathbf{K}_{ff} & \mathbf{K}_{fc} \\ \mathbf{K}_{cf} & \mathbf{K}_{cc} \end{bmatrix} \begin{bmatrix} \mathbf{u}_f \\ \mathbf{u}_c \end{bmatrix} + \begin{bmatrix} 0 \\ m\boldsymbol{I}_2\mathbf{g} + m\boldsymbol{I}_2\mathbf{B} \end{bmatrix} = \begin{bmatrix} \mathbf{F}_f \\ 0 \end{bmatrix}, \tag{83}$$

where the newly introduced vector will be called $\mathbf{N}$, so

$$\mathbf{N} = \begin{bmatrix} 0 \\ m\boldsymbol{I}_2\mathbf{g} + m\boldsymbol{I}_2\mathbf{B} \end{bmatrix}. \tag{84}$$

In order to describe the motion of the pendulum using the same equations of motion, Eq. (60) can be added to the system of equations, where the $\ddot{\theta}$, $\dot{\theta}$, θ and τ terms can be added to the bottom of the $\ddot{\mathbf{u}}$, $\dot{\mathbf{u}}$, $\mathbf{u}$ and $\mathbf{N}$ vectors. Also, the moment of inertia of the pendulum $I = mL^2$, the spring constant k and the damping coefficient b should be added to the bottom right corner of the $\mathbf{M}$, $\mathbf{K}$ and $\mathbf{C}$ matrices respectively. This gives the final equation of motion of

$$\begin{bmatrix} \mathbf{M}_{ff} & \mathbf{M}_{fc} & 0 \\ \mathbf{M}_{cf} & \overline{\mathbf{M}}_{cc} & 0 \\ 0 & 0 & mL^2 \end{bmatrix} \begin{bmatrix} \ddot{\mathbf{u}}_f \\ \ddot{\mathbf{u}}_c \\ \ddot{\theta} \end{bmatrix} + \begin{bmatrix} \mathbf{C}_{ff} & \mathbf{C}_{fc} & 0 \\ \mathbf{C}_{cf} & \mathbf{C}_{cc} & 0 \\ 0 & 0 & b \end{bmatrix} \begin{bmatrix} \dot{\mathbf{u}}_f \\ \dot{\mathbf{u}}_c \\ \dot{\theta} \end{bmatrix} + \begin{bmatrix} \mathbf{K}_{ff} & \mathbf{K}_{fc} & 0 \\ \mathbf{K}_{cf} & \mathbf{K}_{cc} & 0 \\ 0 & 0 & k \end{bmatrix} \begin{bmatrix} \mathbf{u}_f \\ \mathbf{u}_c \\ \theta \end{bmatrix} + \begin{bmatrix} 0 \\ m\boldsymbol{I}_2\mathbf{g} + m\boldsymbol{I}_2\mathbf{B} \\ \tau_z \end{bmatrix} = \begin{bmatrix} \mathbf{F}_f \\ 0 \\ 0 \end{bmatrix}, \tag{85}$$

where τ_z is given by Eq. (55). This equation of motion is used to model the dynamic behaviour of the building in combination with the pendulum TMD system.

I. Newmark-Beta integration method

Using the equations of motion of the building in combination with the TMD system, the dynamic behaviour of the entire structure can be modelled over time. This can be done using a numerical integration method, which is suitable for calculating structural dynamics. The Newmark-beta method is such a suitable method, which was originally developed by Nathan M. Newmark. Newmark suggests that the method is 'capable of application to structures of any degree of complication, with any relationship between force and displacement ranging

from linear elastic behavior through various degrees of inelastic behavior or plastic response, up to failure. Any type of dynamic loading such as that due to shock or impact, vibration, earthquake motion, or blast from a nuclear weapon, can be considered.'[39] The method is proven to be fast and stable, provided that the parameters γ and β are chosen appropriately. Using the Newmark-beta method, the positions and velocities of the building nodes and the angle and angular velocity of the pendulum can be determined over time. This section briefly explains the derivation of the Newmark-beta method, the choice of the Newmark-beta parameters and the use of the Newmark-beta method in the building model.

1) Derivation of the Newmark-beta method
The Newmark-beta method can be derived[39] using the Taylor series, which gives

$$\mathbf{u}_t = \mathbf{u}_{t-\Delta t} + \Delta t \dot{\mathbf{u}}_{t-\Delta t} + \frac{\Delta t^2}{2}\ddot{\mathbf{u}}_{t-\Delta t} + \frac{\Delta t^3}{6}\dddot{\mathbf{u}}_{t-\Delta t} + ..., \quad (86)$$

and

$$\dot{\mathbf{u}}_t = \dot{\mathbf{u}}_{t-\Delta t} + \Delta t \ddot{\mathbf{u}}_{t-\Delta t} + \frac{\Delta t^2}{2}\dddot{\mathbf{u}}_{t-\Delta t} + ..., \quad (87)$$

where the subscript t refers to the current simulation time and the subscript $t - \Delta t$ refers to the simulation time one time step before the current simulation time. Now, the constant in the last term of both equations can be rewritten using β and γ, which gives

$$\mathbf{u}_t = \mathbf{u}_{t-\Delta t} + \Delta t \dot{\mathbf{u}}_{t-\Delta t} + \frac{\Delta t^2}{2}\ddot{\mathbf{u}}_{t-\Delta t} + \beta \Delta t^3 \dddot{\mathbf{u}} + ..., \quad (88)$$

and

$$\dot{\mathbf{u}}_t = \dot{\mathbf{u}}_{t-\Delta t} + \Delta t \ddot{\mathbf{u}}_{t-\Delta t} + \gamma \Delta t^2 \dddot{\mathbf{u}} + ..., \quad (89)$$

where the term $\dddot{\mathbf{u}}$ is defined as

$$\dddot{\mathbf{u}} = \frac{(\ddot{\mathbf{u}}_t - \ddot{\mathbf{u}}_{t-\Delta t})}{\Delta t}. \quad (90)$$

Filling in Eq. (90) into Eqs. (88) and (89) and rewriting the result gives

$$\mathbf{u}_t = \mathbf{u}_{t-\Delta t} + \Delta t \dot{\mathbf{u}}_{t-\Delta t} + \left(\frac{1}{2} - \beta\right)\Delta t^2 \ddot{\mathbf{u}}_{t-\Delta t} + \beta \Delta t^2 \ddot{\mathbf{u}}_t, \quad (91)$$

and

$$\dot{\mathbf{u}}_t = \dot{\mathbf{u}}_{t-\Delta t} + (1-\gamma)\Delta t \ddot{\mathbf{u}}_{t-\Delta t} + \gamma \Delta t \ddot{\mathbf{u}}_t, \quad (92)$$

which are the Newmark-beta equations.

2) β and γ parameters
The β and γ parameters in Eqs. (91) and (92) can be chosen based on the desired behaviour of the integration method, where a trade off has to be made between performance and stability. A value of $\gamma = \frac{1}{2}$[39] has to be chosen to ensure that no positive or negative damping occurs. If $\gamma = 0$, negative damping is present, while for values of $\gamma > \frac{1}{2}$, positive damping is occurs. For a value of $\beta = \frac{1}{4}$, the method uses a uniform acceleration during one time step, where the average between the initial and final acceleration values is taken for this uniform acceleration. For the combination of values $\beta = \frac{1}{4}$ and $\gamma = \frac{1}{2}$, the integration method is unconditionally

stable, which is why these values are chosen for the building model.

3) Solving the displacement over time
In order to solve the displacement of the building and the pendulum system over time, Eqs. (91) and (92) have to be filled in, using the values of $\beta = \frac{1}{4}$ and $\gamma = \frac{1}{2}$ respectively. It can be seen that when using an initial position, velocity and acceleration, the next values in time of these variables can be calculated when the current acceleration is known. The current acceleration is determined using the equation of motion of Eq. (85), where the acceleration can be determined using

$$\ddot{\mathbf{u}} = \mathbf{M}^{-1}(\mathbf{F} - \mathbf{C}\dot{\mathbf{u}} - \mathbf{K}\mathbf{u} - \mathbf{N}) \quad (93)$$

Now, the entire state of the next time step can be determined, where the state vector is equal to

$$\mathbf{u} = \begin{bmatrix} \mathbf{u}_f \\ \mathbf{u}_c \\ \theta \end{bmatrix}, \quad (94)$$

where θ is the pendulum angle and $\mathbf{u}_c$ and $\mathbf{u}_f$ consist of the pendulum connection nodes of the building and the rest of the building nodes respectively. The nodes in both $\mathbf{u}_c$ and $\mathbf{u}_f$ are represented by the three degrees of freedom that are explained in section II-D.

Now, all of the required theory is provided to be able to solve for the displacement of a structure including a pendulum TMD system over time.

III. METHOD
In this section, the modelling and analysis part of the research project is explained into detail. First, the modelling method is explained in section III-A. Next, the dynamic building model of the current Taipei 101 building (using a single TMD), which is constructed based on the theory that is discussed in section II, is explained in sections III-B and III-C. After this, the addition of the MTMD system is discussed in section III-D. Then, the procedure of optimisation of the different models is discussed in section III-E. Finally, the various analysis and comparison methods that are used to validate and compare the models are described in section III-F.

A. Modelling method
For this research project, all of the modelling is done using MATLAB, which means that all of the theory from section II has to be implemented into a MATLAB script. This method of implementing all of the equations from scratch instead of using existing computer software allows for more freedom in the design and analysis of the final building model, although it takes longer to construct the model. When the equations are implemented, changes to the building or the pendulum system can be made easily, since the entire model is available for alteration. This includes general modifications such as layout of the structure, boundary conditions of the model, internal damping of the building etc., but also the fundamental equations that describe the behaviour of the

system. Using MATLAB, detailed analysis can be performed where analysis methods can be constructed from scratch by performing calculations and writing scripts. This also gives freedom for the analysis and comparison phase of the research project, since the amount of different possible analysis and comparison methods is enormous.

The goal is to construct two different models, where one of the models simulates the dynamic behaviour of the current Taipei 101 building including the TMD system as accurately as possible and the other model simulates the dynamic behaviour of a proposed alternative structure, where multiple distributed TMD systems are present. In order to accurately draw a conclusion about the performance of the two different systems, the best configuration of the MTMD system is determined by performing parameter optimisation, which can be done on a large scale due to the freedom of the MATLAB model, as mentioned before. After this optimisation phase, the validation, analysis and comparison of the models leads to a conclusion which points out the system with the best performance based on various factors, which are discussed in section III-F.

B. Assumptions and approximations

In a numerical model, assumptions and approximations have to be made, which allow the simulation to resemble the real system as closely as possible, while keeping the computational costs as low as possible. Various assumptions and approximations of the model are discussed in this section.

1) Building parameters

The Taipei 101 building is resembled by the FEM model shown in Figure 24. When comparing this model with the actual building, shown in Figure 1, it can be seen that the shape of the building model does not exactly match the shape of the real building. An approximation is made where all of the main building dimensions are captured in the building model, i.e. the height of the building, the average height and width of the floor levels, the amount of floors, the material properties etc., are taken into account. However, the changing dimensions per floor are not considered, which means that the building model represents the average dimensions of the real building. Also, steel I-beams are taken to construct the building model, although the actual building consist of a large amount of different materials and constructions. The most important part is that these I-beams can represent the dynamic behaviour of the actual building by matching the natural frequencies of the real building and the building model, as explained in section II-E. Matching this dynamic behaviour and validating the result makes the model sufficient to draw conclusions about the difference in performance of different TMD systems.

2) Initial conditions and boundary conditions

Numerical models require initial conditions to start off the numerical integration calculations over time. As explained in section II-I3, an initial position $\mathbf{u}_0$, velocity $\dot{\mathbf{u}}_0$ and acceleration $\ddot{\mathbf{u}}_0$ are needed for all of the degrees of freedom of the

building nodes. For the pendulum, an initial angle θ_0, angular velocity $\dot{\theta}_0$ and angular acceleration $\ddot{\theta}_0$ are needed. Since no external forces are applied to the pendulum system and the pendulum is set to be stationary in the equilibrium position at $t = 0$, the initial pendulum conditions are equal to zero. In the initial state of the simulation, the building is stationary in the equilibrium position as well, meaning no initial displacement or velocity. The only non-zero initial condition is the wind force on the building, which will cause the building to start moving. To determine the acceleration due to this initial wind force $\mathbf{F}_{f_0}$, Eq. (79) can be filled in using the initial conditions for all variables. This gives

$$\mathbf{M}_{ff}\ddot{\mathbf{u}}_{f_0}+\mathbf{M}_{fc}\ddot{\mathbf{u}}_{c_0}+\mathbf{C}_{ff}\dot{\mathbf{u}}_{f_0}+\mathbf{C}_{fc}\dot{\mathbf{u}}_{c_0}+\mathbf{K}_{ff}\mathbf{u}_{f_0}+\mathbf{K}_{fc}\mathbf{u}_{c_0} = \mathbf{F}_{f_0},$$
(95)

where $\dot{\mathbf{u}}_{f_0} = \mathbf{0}$, $\dot{\mathbf{u}}_{c_0} = \mathbf{0}$, $\mathbf{u}_{f_0} = \mathbf{0}$, $\mathbf{u}_{c_0} = \mathbf{0}$ and $\mathbf{N}_0 = \mathbf{0}$. Therefore, the equation can be reduced in size because of the zero-vectors. This gives

$$\mathbf{M}_{ff}\ddot{\mathbf{u}}_{f_0} + \mathbf{M}_{fc}\ddot{\mathbf{u}}_{c_0} = \mathbf{F}_{f_0},$$
(96)

which can be rewritten to give

$$\begin{bmatrix} \mathbf{M}_{ff} & \mathbf{M}_{fc} \end{bmatrix} \begin{bmatrix} \ddot{\mathbf{u}}_{f_0} \\ \ddot{\mathbf{u}}_{c_0} \end{bmatrix} = \mathbf{F}_{f_0},$$
(97)

where

$$\begin{bmatrix} \ddot{\mathbf{u}}_{f_0} \\ \ddot{\mathbf{u}}_{c_0} \end{bmatrix} = \ddot{\mathbf{u}}_0.$$
(98)

Therefore, the initial acceleration due to the initial wind force $\mathbf{F}_{f_0}$ can be determined using

$$\ddot{\mathbf{u}}_0 = \begin{bmatrix} \mathbf{M}_{ff} & \mathbf{M}_{fc} \end{bmatrix}^{-1} \mathbf{F}_{f_0},$$
(99)

which means that the initial conditions of the model are equal to

$$\ddot{\mathbf{u}}_0 = \begin{bmatrix} \mathbf{M}_{ff} & \mathbf{M}_{fc} \end{bmatrix}^{-1} \mathbf{F}_{f_0}, \qquad \ddot{\theta}_0 = 0,$$
$$\dot{\mathbf{u}}_0 = \mathbf{0}, \qquad\qquad\qquad \dot{\theta}_0 = 0, \qquad (100)$$
$$\mathbf{u}_0 = \mathbf{0}, \qquad\qquad\qquad \theta_0 = 0.$$

where $\mathbf{F}_{f_0} = f(0)$, where $f(0)$ is a discrete function that describes the wind force on all of the building nodes at a time of $t = 0$.

3) Wind force model

In order to apply a realistic wind force to the building model, ideally, the local climate and environment around the building is taken into account, as well as effects such as vortex shedding and the increase of wind velocity with height. However, to determine the difference in dynamic behaviour of the different TMD systems, a more simple wind force model is sufficient, since the behaviour of the TMD systems can be analysed most accurate in free vibration. Therefore, two different wind models are created. One of the wind models is a randomly generated, more realistic wind model that can be used to represent the real environment and circumstances to which the different building models can be exposed. The other wind model is a simpler model, where the wind force will be removed after a certain amount of simulation time, such that the behaviour of the TMD systems can be analysed in free vibration.

First, the more realistic wind model is explained. Around the Taipei 101 building, typhoons can occur that cause large wind gusts, where the wind velocity during a strong typhoons (typhoon Soulik) was measured to be at an average of $15.24m/s$[40], measured over a time period of 21 hours at a height of $h_0 = 15m$. A random wind force model is made where the velocity v_0 of the wind is constructed from multiple sinusoids with random frequencies chosen from a certain frequency range. The wind is chosen to come from one side of the building, since wind directions usually do not change suddenly. The magnitude of the wind velocity has a maximum value of $15.24m/s$, where the frequencies of the wind force are chosen such that this maximum velocity is not present for more than around $3s$, in order to most accurately represent wind gusts. This constructed wind velocity is created for a height of $15m$ above ground level. An example of such a randomly generated wind velocity function is shown in Figure 7.
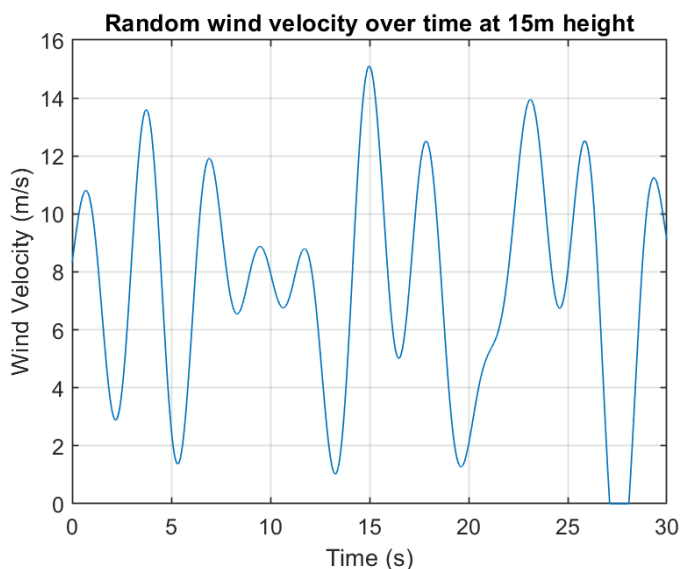

Fig. 7: Randomly generated wind velocity function using sinusoids.

Wind velocities increase in height according to the Hellmann exponent law[41], which is given by

$$v = v_0 \left(\frac{h}{h_0} \right)^\alpha, \tag{101}$$

where v is the wind velocity at height h, v_0 is the wind velocity at height h_0 (which is usually a height of $10m$) and α is the Hellmann exponent, which is a coefficient that depends on the surroundings of the measurement point. A value of $\alpha = 0.14$[42] is often used as a standard value for most situations, where the wind is not affected by any surrounding structures or the environment. Since the Taipei 101 building is not located in a mountain environment and rises far above all of the surrounding buildings, as also shown in Figure 1, the value of $\alpha = 0.14$ is considered to be appropriate to use for the wind model. Now, when filling in the randomly generated wind velocity function v_0, the height $h_0 = 15m$ at which this

velocity is present and the coefficient α, the wind velocity function v can be determined over time for different heights h. In order to apply a wind force on the nodes of the building, the wind velocity at the nodes of the building has to be known. Therefore, the wind velocity function v is calculated for all of the heights of the building nodes to which a wind force will be applied. An example of a velocity distribution at $t = 15s$, taken from the wind velocity function shown in Figure 7, is shown in Figure 8.
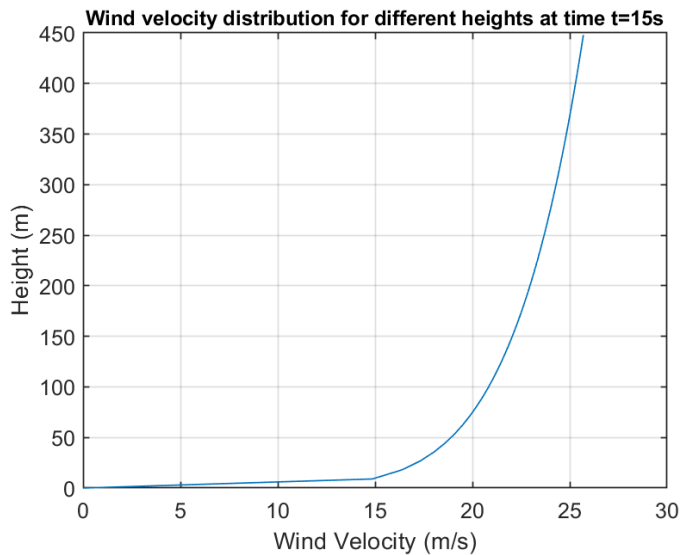

Fig. 8: Wind velocity distribution at $t = 15s$, using the randomly generated wind velocity function at $h_0 = 15m$ shown in figure 7.

Now, these velocity functions have to be transformed into forces on the corresponding building nodes, which can then be assigned to the same nodes in the vector $\mathbf{F}_f$ to be applied to the building. The force on one of the nodes of the building can be calculated using

$$F = \frac{1}{2} \rho v^2 A, \tag{102}$$

where ρ is the air density, which is taken to be $\rho = 1.225 kg/m^3$ (air density at sea level) and A is the surface area of the building where the wind is acting on. This surface area can be determined by taking the area around one node, where the area of each node will correspond to half of the area of the wall of the floor above and half of the area of the wall of the floor below. This means that the area of each of the building nodes will just be each to the area of the wall of one floor, which is the height of one floor multiplied by the width of one floor. A constraint is set to for a height of $h = 0$, such that the wind velocity and thus the wind force is equal to zero for the bottom nodes of the building. For the top node of the building, there is no floor above, which means that the area on which the wind velocity acts for this node is half of the area that is used for the other nodes. Therefore, the force on this node is divided by 2. The effect of vortex shedding is neglected since it is considered to be out of the scope of the research project and not necessary for performing a comparison of the different TMD systems.

Secondly, the more simple wind model is explained. For this model, a constant wind velocity of $v_0 = 15.24 m/s$ is used, which is converted to a velocity distribution for different heights using Eq. (101) in the same way as the more realistic wind model. Then the found wind velocities at the building nodes are converted to forces using Eq. (102). The same constraint is used for a height of $h = 0$ as in the more realistic wind model and also, the force on the top node is divided by 2. This wind model is not random, which makes it appropriate to use for the analysis part of the research project, since both TMD systems should be simulated using the same circumstances and thus the same external wind forces. After a simulation time of $t = 3s$, this force is removed, which ensures that the TMD systems can be compared in free vibration.

4) Time step
The numerical simulation of the dynamic building motion is a discrete simulation, which means that it requires a time step, after which each calculation of the new variables of the system is performed. The time step Δt is used in the Newmark-beta equations shown in section II-I1 and should be chosen small enough such that the numerical integration error stays low enough, but the computation time is within an acceptable margin, such that the simulations can be performed. However, for the values of $\beta = \frac{1}{4}$ and $\gamma = \frac{1}{2}$, which are used in the building model, the integration method is unconditionally stable. Therefore, the time step of the building model should be determined based on the natural frequencies of the building, where the highest natural frequency determines the step size using

$$\Delta t \leq \frac{1}{f_{max}}, \tag{103}$$

where f_{max} is the highest eigenfrequency of the building structure. Choosing the time step according to Eq. (103) ensures that the simulation is fast enough to capture all of the dynamics of the system. Using the eigenvalue study, the highest eigenfrequencies of the single TMD and MTMD building models are found to be $144.15 Hz$ and $285.21 Hz$ respectively, so the time step should be chosen according to

$$\Delta t \leq \frac{1}{144.15} = 0.0069372s \tag{104}$$

and

$$\Delta t \leq \frac{1}{285.21} = 0.0035062s, \tag{105}$$

respectively. The chosen time step is equal to $\Delta t = 0.001s$ for both models to ensure appropriate behaviour and prevent divergence. A small time step convergence study is performed from which is concluded that the system behaviour is converged for this time step, which means that the time step is chosen small enough to accurately represent the dynamic system behaviour.

C. Modelling procedure
The structure of the model is briefly explained in this section. Each part of the model is only addressed briefly, since most parts are extensively explained in the theory discussed in previous sections.

1) Building initialisation
The first step of the building model is the initialisation of the nodes of the building, along with the properties of the building and the TMD system or the MTMD system. The nodes of the building are initialised in an array, denoting the initial x- and y-location and the initial change in motion in the x-direction. These are the degrees of freedom per node, as explained in section II-D.

2) Element connectivity
Next, a connectivity matrix $\mathbf{A}$ is made, which is an $n \times n$ matrix, where n is the amount of nodes of the FEM structure, such that the row and column numbers correspond to the separate nodes of the structure. Now, when the combination of a certain row and column of the matrix represents two nodes that should be connected with a beam element in the FEM model, this value in the matrix should be set equal to $\mathbf{A}_{ij} = 1$, where i and j represent the row and column of the nodes in question. For a combination of a row and column of the matrix that represents two nodes that should not be connected with a beam element in the FEM model, the corresponding value in the matrix should be set equal to $\mathbf{A}_{ij} = 0$. This way, a matrix is constructed which contains the information whether two nodes are connected in the FEM model or not. Using this matrix, the global stiffness and mass matrices can be constructed, by adding the local stiffness and mass matrices only to the locations in the global stiffness and mass matrices where two nodes should be connected by a beam element, so where $\mathbf{A}_{ij} = 1$.

3) Stiffness, mass and damping matrices
Next, the local stiffness and mass matrices are constructed, which results in the matrices shown in Eqs. (21) and (22). Multiple different matrices are constructed, since the length of a beam element L is not the same for all beam elements of the structure. Next, these stiffness and mass matrices are transformed as explained in section II-D3, where different angles of θ are used depending on the angle with which the beam element should be rotated to align with the global coordinate system. Then, the global stiffness and mass matrices are constructed as explained in section II-D4, also using the connectivity matrix $\mathbf{A}$. Using these global stiffness and mass matrices, the global damping matrix is constructed using Rayleigh damping, as explained in section II-F. Then, the TMD mass or multiple TMD masses are added to the global stiffness, mass and damping matrices, as explained at the end of section II-H4.

4) Boundary conditions
The following step is adding boundary conditions to the building model. The boundary conditions implemented in the building model make sure that the building is fixed to the ground, where the ground is assumed to be stationary. As can be seen in Figure 24, the building model is connected to the ground using two nodes. The boundary conditions are applied to both of these nodes and are equal to

$$u_1 = u_2 = 0, \quad \dot{u}_1 = \dot{u}_2 = 0 \quad and \quad \ddot{u}_1 = \ddot{u}_2 = 0, \tag{106}$$

which are implemented in the model by setting the 6×6 sub-matrices that correspond to the 6 degrees of freedom to the bottom two nodes in the stiffness, mass and damping matrices equal to a 6×6 identity matrix (I_6). Also, no external forces are applied to these bottom nodes. The combination of these measures ensures that no acceleration is applied to the bottom nodes, which means that no displacement or velocity is induced for these nodes. This means that the boundary conditions shown in Eq. (106) are realised.

5) Iteration scheme

Finally, the iteration scheme is used to determine the dynamic behaviour over time. The iteration scheme uses the Newmark-beta method, as explained in section II-I. First, the iteration scheme should be initialised. This is done by assigning the Newmark-beta parameters β and γ and initialising all of the required vectors used in the iteration loop. This also includes setting the initial conditions of the model, shown in Eq. (100). Next, the wind force distribution along the building height over time is constructed as explained in section III-B3. Using the initial wind force and the other initial conditions, the initial acceleration is determined with which the iteration scheme can be started, using Eq. (93).

In the iteration scheme, the external wind force is updated, after which the torque of the pendulum is calculated, as explained in section II-H2. Next, the force from the pendulum on the connection nodes is determined as explained in section II-H4, after which these forces and the torque of the pendulum are applied to the corresponding locations in the **N** vector. Then, the Newmark-beta equations are used to solve for the displacement of the entire model structure, as explained in section II-I1. In Eqs. (91) and (92) can be seen that apart from the variables at time $t - \Delta t$, the acceleration from the current time t is required to calculate the current position $\mathbf{u}_t$ and velocity $\dot{\mathbf{u}}_t$ vectors. This can be done by calculating a prediction for the position and velocity vectors without including the current acceleration terms. This gives

$$\mathbf{u}_{pred} = \mathbf{u}_{t-\Delta t} + \Delta t \dot{\mathbf{u}}_{t-\Delta t} + \left(\frac{1}{2} - \beta \right) \Delta t^2 \ddot{\mathbf{u}}_{t-\Delta t} \quad (107)$$

and

$$\dot{\mathbf{u}}_{pred} = \dot{\mathbf{u}}_{t-\Delta t} + (1 - \gamma) \Delta t \ddot{\mathbf{u}}_{t-\Delta t}, \quad (108)$$

after the value for the current acceleration $\ddot{\mathbf{u}}_t$ can be calculated using $\mathbf{u}_{pred}$ and $\dot{\mathbf{u}}_{pred}$, which gives

$$\ddot{\mathbf{u}}_t = \mathbf{M}^{-1} (\mathbf{F} - \mathbf{C} \dot{\mathbf{u}}_{pred} - \mathbf{K} \mathbf{u}_{pred} - \mathbf{N}). \quad (109)$$

Using this current acceleration, the final current position $\mathbf{u}_t$ and velocity $\dot{\mathbf{u}}_t$ vectors can be calculated according to

$$\mathbf{u}_t = \mathbf{u}_{pred} + \beta \Delta t^2 \ddot{\mathbf{u}}_t \quad (110)$$

and

$$\dot{\mathbf{u}}_t = \dot{\mathbf{u}}_{pred} + \gamma \Delta t \ddot{\mathbf{u}}_t, \quad (111)$$

which include the new positions and velocities of the building and the new angle θ and angular velocity $\dot{\theta}$ of the pendulum respectively, according to the Newmark-beta equations. Finally, the new pendulum positions are calculated by filling in the

found pendulum angle θ in Eqs. (61) and (62), which give the displacement of the pendulum mass in the global coordinate system in the x- and y-direction respectively.

D. Multiple TMD system

A second model is made, where 3 TMD systems are implemented instead of a single TMD system. In order to add multiple TMD systems to the model, the same modelling produce has to be followed as explained in section III-C, except for the fact that every pendulum variable should be implemented 3 times to represent the three different systems. The TMD systems are attached alongside each other at the same building height at horizontal locations of $\frac{1}{6}L_w$, $\frac{1}{2}L_w$ and $\frac{5}{6}L_w$, where L_w is the width of the building. This is done to obtain symmetry in the beam elements with which the attachment points are connected to the building, such that the same behaviour is obtained when the attachment point moves to the right as when the attachment point moves to the left. This symmetry can be seen in Figure 9, where the MTMD system configuration is shown in detail.
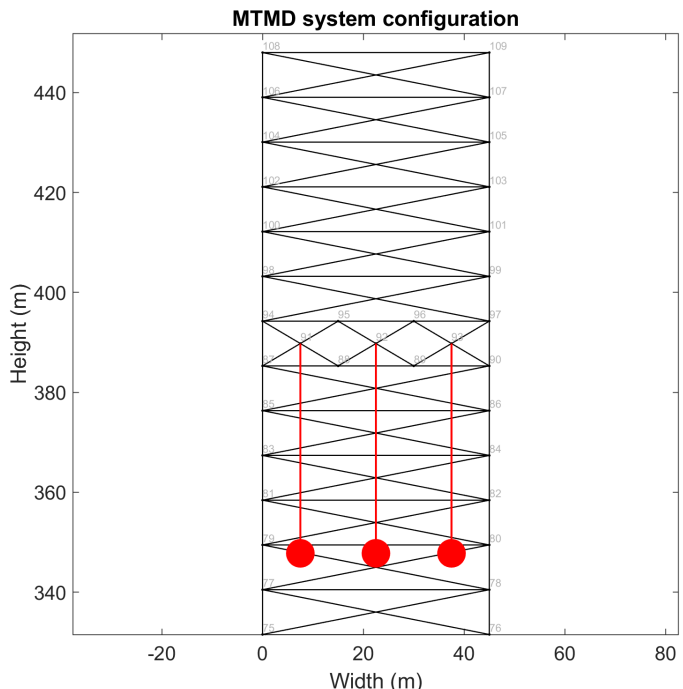

Fig. 9: MTMD system configuration

The rest of the building model is the same as for the single TMD system, as shown in Figure 24. While the lengths of the pendulums are kept equal, the spring constants k are set to different values for each pendulum TMD system. This makes each of the pendulums oscillate at a slightly different frequency, which leads to a larger frequency bandwidth for which the building vibration can be mitigated.

E. Parameter optimisation

Now, both TMD systems should be optimised according to the most appropriate optimisation strategy. For the single TMD system, the optimisation consists of tuning the pendulum

TMD parameters such that the system of the Taipei is represented as closely as possible. For the MTMD system, the frequency of the different pendulums should be tuned such that the optimal frequency operation bandwidth is obtained, where the robustness of the system is improved while the oscillation frequencies are also chosen to be close enough to the fundamental oscillation frequency such that the suppression performance is not reduced too much. The derivation and tuning of the building and pendulum TMD natural frequencies is explained in section II-F and II-H3 respectively.

1) Single TMD system

For the single TMD system model, the length of the pendulum cable is set equal to the length of the pendulum cable in the actual Taipei 101 building, which equals $42m$[37]. Now, Eq. (58) can be rewritten to give

$$k = mL^2(2\pi f)^2 - mgL, \tag{112}$$

such that the torsional pendulum stiffness can be determined. When filling in the length of $L = 42m$, the pendulum mass $m = 660998kg$, the required fundamental oscillation frequency $f = 0.1043Hz$ and the gravitational constant g, the required spring constant to tune the TMD to the correct natural frequency is found to be $k = 228412534Nm/rad$. The correct attachment height of the TMD system is approximated by the height at which the TMD system is attached in the actual building, which is at $390.60m$[29]. In the building model, the exact height at which the TMD system is attached is equal to $389.76m$. Using this configuration, also shown in Figure 24, the analysis of the single TMD system model is performed. Now, the damping coefficient can be calculated using Eq. (59), which gives a value of $b = 309642423Nm \cdot s/rad$.

2) MTMD system

For the MTMD system model, the lengths of the different TMD systems are set equal to the length of the single TMD system and the pendulums are attached at an equal height, as mentioned in section III-D. Also, the mass of the single TMD system is distributed among the three MTMD systems. The mass of the building is tuned such that 0.24% of the mass of the building gives the mass of the three pendulum systems combined, which should be approximately equal to $660000kg$. In the MTMD system model, the mass of each of the MTMD pendulum masses is equal to $m = 220377kg$. The different eigenfrequencies can be obtained by calculating the required torsional spring constants of the systems using Eq. (112). However, after calculating the theoretically required values for the MTMD system, a study is performed which determines the most appropriate pendulum TMD parameters. This can be done using a parameter sweep, where multiple pendulum parameters will be analysed simultaneously to find the most appropriate combination for which the MTMD system performance is most optimal.

The parameters that are optimised in this study are the spring constant k, the damping coefficient b and the attachment height h of all of the pendulums, where the pendulums are all attached to the same height h.

Parameter sweep 1

In a first study, all of the MTMD systems will be set to have the same spring constant k and damping coefficient b, after which the bandwidth of the system and thus the different values for the spring constant k and damping coefficient b will be analysed in a separate study. In order to perform an accurate and detailed parameter sweep, reasonable initial values should be chosen for the parameters, around which the sweep will be performed. The initial value for the spring constants can be determined by filling in the mass of $m = 220377kg$ one of the TMD systems into Eq. (112), while keeping the rest of the parameters the same as before. This gives an initial spring constant of $k = 76152789Nm/rad$ for all of the TMD systems in the first study. This spring constant corresponds to a natural frequency of $f = 0.1043Hz$. Now, the corresponding damping coefficient can be filled in by filling in the found parameters into Eq. (59), which gives an initial damping coefficient of $b = 103234852Nm \cdot s/rad$ for all of the TMD systems. Finally, the initial attachment height h of all of the pendulums will be the same as in the single TMD system model, which is at a height of $389.76m$.

Also, a range and step size should be assigned to each of the parameters, which indicates the list of parameters that should be used as input for the optimisation study. The chosen ranges for the study are equal to $k = 74237480.99Nm/rad - 78079147.42Nm/rad$, $b = 101928362.28Nm \cdot s/rad - 104532410.18Nm \cdot s/rad$ and $h = 371.84m - 443.52m$, where the ranges of k and b are divided into 5 values and the range of h is divided into 9 values, which are equally distributed along the range, starting and ending on the mentioned values.

Now, in order to determine the performance of these combinations of parameters, an objective function should be constructed, which should become as low as possible. The maximum displacement of the nodes of the building should be as low as possible, which means that this variable can be used. The displacement in the x-direction is dominant in the FEM model, which is why the objective function is set equal to

$$f(u_x) = \sum_{i=1}^{n} \mathbf{u}_{x,i}^2, \tag{113}$$

where $\mathbf{u}_{x,i}$ is the displacement of the ith node of the building in the FEM structure in the x-direction.

Using the mentioned parameters, a sweep is performed where the dynamic building motion is simulated over time for all of the parameter combinations. The maximum deflection and the corresponding value of the objective function are stored for each simulation, after which the minimum value for the objective function can be found. The corresponding combination of parameters therefore results in a lower maximal displacement than all of the other combinations.

This means that the most optimal parameter combination of the input parameters is found. It was found that the most optimal attachment height for the MTMD system was as high as possible in the building model. However, in order to be able to compare the performance of the TMD and the MTMD system based on the feature of having multiple TMD systems and not based on the attachment height, the value of h is kept the same as for the single TMD system. Nevertheless, this is result should be noted, since placing the TMD system even higher in the Taipei 101 building would increase the suppression abilities of the system, according to the parameter sweep result. The found optimal values of k and b and the chosen value of h are shown in Table IV.

k (Nm/rad)	b ($Nm \cdot s/rad$)	h (m)
76152789	103234852	389.76

TABLE IV: Results of the first MTMD system parameter optimisation study.

Now, the result of the sweep is refined, by taking the values shown in Table (IV) as the new initial values and setting new parameter ranges of $k = 75513125Nm/rad - 76793681Nm/rad$, $b = 102800365Nm \cdot s/rad - 103668347Nm \cdot s/rad$, where the range is divided into 5 values which are equally distributed along the range. This results in the refined optimal parameters that are shown in Table V.

k (Nm/rad)	b ($Nm \cdot s/rad$)	h (m)
76152789	103234852	389.76

TABLE V: Refined results of the first MTMD system parameter optimisation study.

It can be seen that exactly the same values are found as are used for the single TMD system. This is because the single TMD system is perfectly tuned to the building oscillation. Therefore, it is expected that these values are the same for the MTMD system as well, when no bandwidth is used for the system. This provides a good model validation. It was found that when lowering the value of k, the suppression ability of the pendulum system was better in the first few oscillations, but became worse over time. Therefore, tuning the frequency exactly to the building frequency resulted in slightly less performance in the first oscillations, but better performance overall.

Parameter sweep 2

A second study can be performed, using the values shown in Table V. In this study, the MTMD systems are set to different values for the spring constant k and damping coefficient b, in order to determine the most optimal frequency bandwidth to which the TMD systems should be tuned. Two parameters Δk and Δb are used to determine the optimal parameters, where one of the outer TMD systems will be tuned to a value of $k_{initial} + \Delta k$ and the other outer TMD system will be tuned to a value of $k_{initial} - \Delta k$, which means that the difference between the spring constant and damping coefficient between adjacent TMD systems will be the same, which provides a symmetrical frequency bandwidth around the fundamental oscillation frequency.

The initial value for the spring constants can be determined based on the found spring constant in Table V and will be equal to $k = 76152789Nm/rad$ for the centre TMD system. This spring constant corresponds to a natural frequency of $f = 0.1043Hz$. The other systems will be tuned initially to the same frequency of $f = 0.1043Hz$ and will then be decreased and increased gradually to the frequencies of $f = 0.1023Hz$ and $f = 0.1063Hz$ respectively, in order to determine the behaviour of the system for different bandwidths. These values are chosen by considering the average change in natural frequency of the Taipei 101 building in both translational building directions (East-West and North-South), measured[10] over a period of one year. The average measured frequency variations in the directions Earth-West and North-South are 1.006% and 2.771% respectively. The average of these values is equal to 1.889%. When taking 1.889% of the natural frequency of the building model, the average natural frequency variation becomes $0.00197Hz$, which is why this change in natural frequency is chosen as the maximal change to both directions for the MTMD systems in the parameter sweep. Therefore, using Eq. (112) and filling in the same parameters as before, using the frequencies of $f = 0.1023Hz$ and $f = 0.1063Hz$, gives maximal spring constant values of $k_1 = 69811300Nm/rad$ and $k_3 = 82616955Nm/rad$ respectively for the two other TMD systems. Now, using Eq. (59), the corresponding maximal damping coefficient values are found to be $b_1 = 98843157Nm \cdot s/rad$ and $b_3 = 107527123Nm \cdot s/rad$.

The initial parameter sweep values of k and b are equal to the values shown in Table V for all TMD systems. Since the most appropriate bandwidth is determined in this study, only the parameters of the outer two TMD systems will be used as input for the study. The used range of the study parameters is $\Delta f = 0Hz - 0.0020Hz$. This translates to absolute ranges of $k_1 = 76152789Nm/rad - 69811300Nm/rad$, $k_3 = 76152789Nm/rad - 82616955Nm/rad$, $b_1 = 103234852Nm \cdot s/rad - 98843157Nm \cdot s/rad$ and $b_3 = 103234852Nm \cdot s/rad - 107527123Nm \cdot s/rad$, where the values for the centre TMD system remain the same.

The performance of the system is monitored using the same objective function shown in Eq. (113) by simulating the dynamic building motion over time. However, for this sweep, the measured[10] average natural frequency variation of the building is taken into account, as described before, which means that the building model will be off-tuned to a natural frequency of $0.1023Hz$, to simulate the short term or long term change in natural frequency (off-tuning) of the building.

The result of this second parameter sweep is that the MTMD system works best when the TMD systems are all tuned exactly to the original fundamental frequency of the building model of $0.1043Hz$, even when the building model

is off-tuned to a natural frequency of $0.1023Hz$. Therefore, according to the parameter sweep, the best parameters for all of the TMD systems in the MTMD system are found to be equal to the values shown in Table V. In sections IV and V, this behaviour will be analysed. Therefore, the parameters of the MTMD system where chosen based on the average natural frequency variation of the building, which was found to be 1.889%, as explained before. The chosen values would theoretically make sure that the bandwidth of the MTMD system would be bigger, where the outer masses are tuned to a frequency that corresponds to the average natural frequency variation of the building in positive and negative direction. This bandwidth would in theory suppress the vibration of an off-tuned building slightly better than the system without bandwidth. To test this behaviour and potentially disprove this theory, the MTMD system is tuned to have the bandwidth $0.1023Hz - 0.1063Hz$. The corresponding parameters of the two outer TMD systems are shown in Table VI.

k$_1$(Nm/rad)	k$_3$(Nm/rad)	b$_1$(Nm·s/rad)	b$_3$(Nm·s/rad)
69811300	82616955	98843157	107527123

TABLE VI: Chosen parameters of the two outer TMD systems, based on the second MTMD system parameter optimisation study.

Combining the two parameter sweep studies gives the final MTMD system parameters, which are shown in Table VII. Note that the TMD systems are numbered from left to right according to Figure 9.

k$_1$(Nm/rad)	k$_2$(Nm/rad)	k$_3$(Nm/rad)
69811300	76152789	82616955

b$_1$(Nm·s/rad)	b$_2$(Nm·s/rad)	b$_3$(Nm·s/rad)	h (m)
98843157	103234852	107527123	389.76

TABLE VII: Final results of the two MTMD system parameter optimisation studies.

F. Method of analysis techniques

In order to determine the performance of the single TMD and the MTMD systems, analysis techniques should be determined, which requires two steps. First, both models should be validated such that it is clear that the models behave as required, after which both systems should be assessed and compared based on the suppression ability, robustness, space usage and off-tuning mitigation.

1) Model validation

The model validation methods that will be used are explained in this section. First, modal analysis will be performed, where the mode shapes of the found eigenvectors and the corresponding eigenfrequencies of the three most significant modes are compared to experimental values. This is done using an eigenvalue study, in the same way as explained in section II-F. Also, the frequency response of the dynamic building motion will be made. To do this, the fast Fourier transform (FFT) is taken for the displacement function in

x-direction over time for all of the building nodes. All of the frequency responses are shown in one plot, which gives a general overview of the frequencies that are present in the building structure during dynamic motion. Then, the dominant frequencies will be compared with the frequencies found in the modal analysis. Finally, the small angle approximation used for the pendulum system will be validated.

2) Model comparison

The methods that are used to compare the performance of the single TMD and the MTMD systems based on suppression ability, robustness, space usage and off-tuning mitigation are explained in this section. The main comparison method to monitor the suppression ability of the systems will consist of comparing the building deflection after an equal external wind load is applied for a period of $3s$, after which the two systems are analysed in free vibration. For the suppression ability comparison, a third model will be added, which does not include a TMD system. This is done to be able to see the effect of a mass damper in general and be able to compare the two different types of mass dampers at the same time. The average maximum building deflection per floor will be shown, which is done by taking the maximum deflection of the building for every half-period over time and taking the average of all of these maximum deflections. This will thus not be the absolute maximum deflection of the building, but this does provide a good comparison method, because the result of the average maximum deflection for each of the models is not taken only for a single moment in time but for the entire oscillation, thus showing the average behaviour of the model over the entire simulation period. Also, the motion in x-direction of the attachment point(s) and the pendulum mass(es) of the models will be shown over time.

In order to test the robustness and off-tuning mitigation of the systems, the building model is adjusted such that the natural frequencies of the building are slightly different to simulate a temporary or permanent change in natural frequency of the building. The natural frequencies of the first three oscillation modes of the building that are used in this comparison method are shown in Table VIII.

	Mode 1	Mode 2	Mode 3
Natural frequencies single TMD (Hz)	0.1023	0.5647	0.9367
Natural frequencies MTMD (Hz)	0.1023	0.5650	0.9367

TABLE VIII: Off-tuned natural frequencies of the building models, used to simulate a temporary or permanent change in natural frequency of the building.

Using these natural frequencies, the displacement per floor will be shown for the moment in time where the building deflection is maximal for both the single TMD system and the MTMD system.

Finally, a conclusion will be drawn regarding the space usage of both TMD systems, based on the dimensions used in both models and the other possible implementations of both systems in terms of space usage.

3) Model behaviour using realistic wind model
In order to show a more realistic building model behaviour, a more realistic wind force should be applied. The more realistic random wind model, as explained in section III-B3, is applied to the single TMD system in order to show how the building would roughly behave in real life. Although the simpler constant wind force model provides a good method for model comparison, the more realistic model provides insight in how the building would behave when exposed to a more realistic wind force.

IV. RESULTS

In this section, the results of the analysis techniques discussed in section III-F are shown and briefly explained. The results are discussed in section V.

A. Model validation results

The results of the different methods to validate the behaviour of the building models are shown in this section.

1) Modal analysis
Using the eigenvalue study as explained in section II-F, the eigenvectors for the three most significant oscillation modes of the building could be plotted. The mode shapes of the single TMD system and the MTMD system models are shown in a single plot in Figure 10.

(a) Mode 1   (b) Mode 2   (c) Mode 3
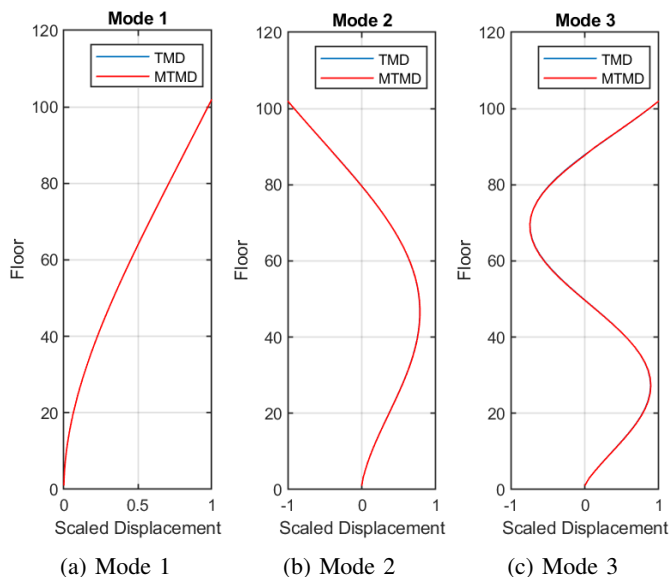
Fig. 10: Eigenvectors (mode shapes) of the single TMD and MTMD system.

Note that the mode shapes of the TMD system and the MTMD system are almost the same. This will be discussed in section V-B1. The corresponding eigenfrequencies of the single TMD system and the MTMD system models are shown in Table IX.

	Mode 1	Mode 2	Mode 3
Eigenfrequencies single TMD (Hz)	0.1043	0.5756	0.9548
Eigenfrequencies MTMD (Hz)	0.1043	0.5759	0.9547

TABLE IX: Eigenfrequencies of the single TMD and MTMD building models.

2) Frequency response
The frequency response of the x-displacement of all of the building nodes over time is constructed for both the single TMD system and MTMD system models. The frequency responses of all of the different building nodes are plotted in a single plot, which creates an overview of all of the frequencies that are present in the entire system. These frequency responses are plotted for the single TMD system and the MTMD system models in Figures 11 and 12 respectively.
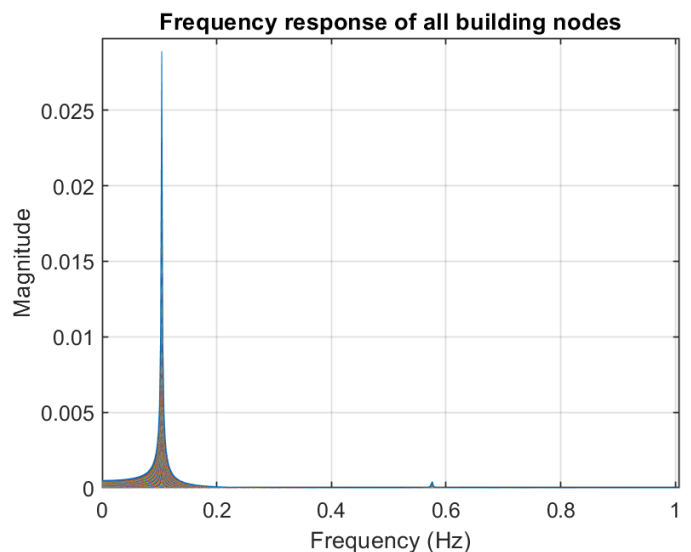

Fig. 11: Frequency response of all building nodes of the single TMD system.
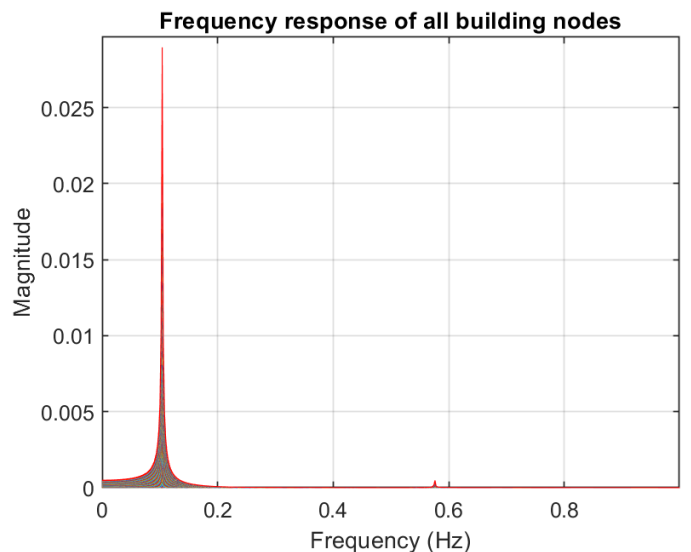

Fig. 12: Frequency response of all building nodes of the MTMD system.

It can be seen that Figures 11 and 12 both show almost the same frequency response. The frequency peaks for both responses are located at $0.1040Hz$ and $0.5753Hz$, where the peak are $0.5753Hz$ is almost negligible in height compared to the peak at $0.1040Hz$. No peak is visible around the eigenfrequency of mode 3 for both systems as shown in Table IX. This peak is present in both plots, but is too small to see.

3) Small angle approximation

The small angle approximation validation is performed by plotting the angle θ of the pendulum together with the x-displacement of the pendulum over time, for the situation where a wind velocity of $32.78m/s$[38] is applied at a building height of $10m$. This corresponds to the wind velocity distribution that was chosen as a maximum wind velocity, meaning that this wind velocity would be the highest that the building would ever be exposed to. For this wind velocity, the pendulum damping was designed to have a maximum swing of $1.50m$, as explained in section II-H3. Figure 13 shows the pendulum angle θ and the x-displacement of the pendulum over time for this situation, which thus contains the maximum values for the pendulum angle θ and the x-displacement of the pendulum that the system will ever experience.
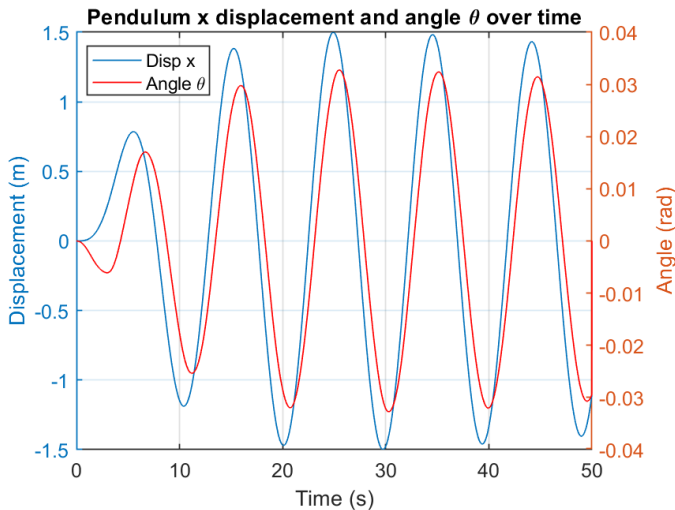

Fig. 13: Small angle approximation validation for the maximum excitation of the pendulum TMD system.

The maximum value of the pendulum angle is found to be $\theta = 0.0328rad$ at a time of $t = 25.50s$.

B. Model comparison results

The results of the different methods to compare the behaviour of the building models are shown in this section.

1) Suppression ability

The suppression ability of the different building models is shown in two different ways. For this comparison method, three different building models are analysed, namely the model using the single TMD, the model using the MTMD and the model using no TMD, as explained in section III-F2. First, the time response of the different models is constructed. This

is done by plotting the x-displacement of the attachment point(s) and the mass(es) of the system over a time period of $t = 0s - 500s$ for the TMD and MTMD systems and by plotting the x-displacement of the attachment point without a TMD mass attached for the system without a TMD over the same time period. The results are shown in Figures 14, 15 and 16 for the TMD, MTMD and 'no TMD' models respectively.
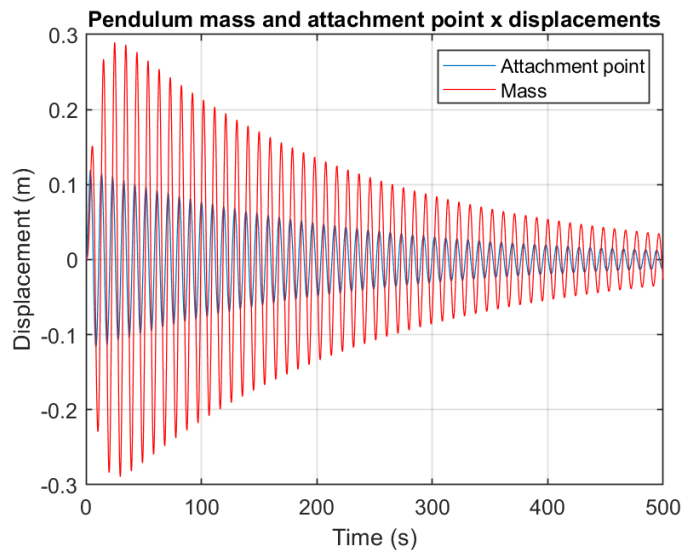

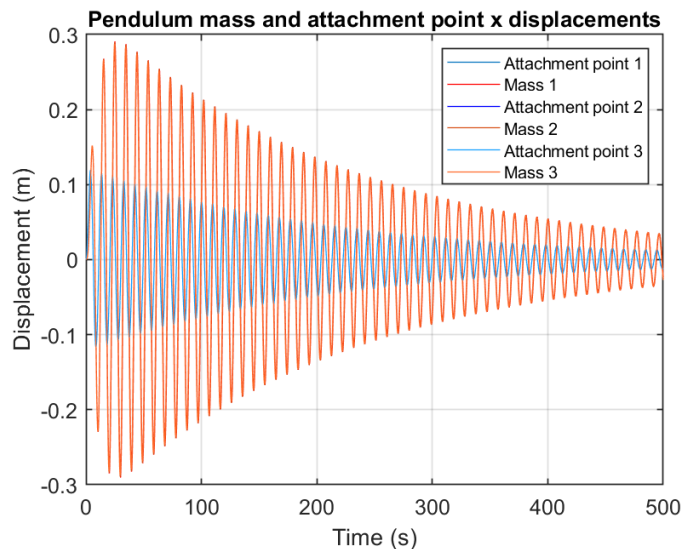Fig. 14: Time response of the single TMD system.

Fig. 15: Time response of the MTMD system.

Note that for the time response of the MTMD system, shown in Figure 15, all three attachment points and pendulum masses are shown. However, since these are close together, this is not clearly visible. A zoomed in version of this time response is shown in Figure 18.
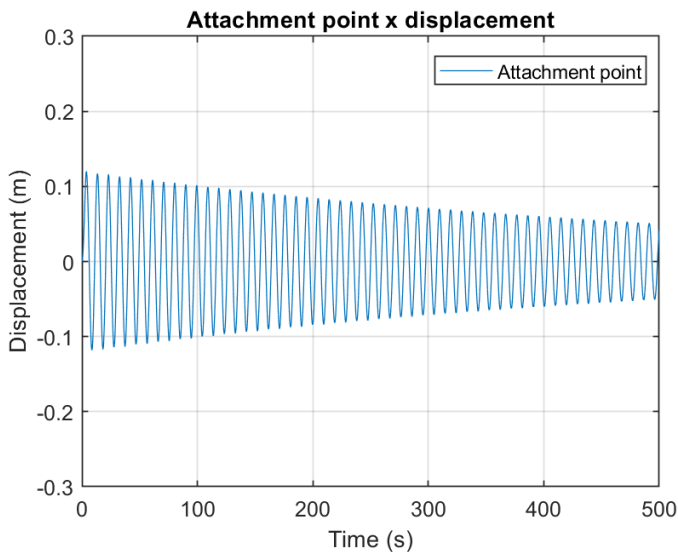
Fig. 16: Time response of the system without TMD.

The second comparison method for the suppression ability of the models is performed by taking the average maximal deflection, which is done by taking the maximal deflection of the building each half-period over the entire simulation time and taking the average of these maximum deflections, as explained in section III-F2. The average maximum deflections of the three different models are shown in Figure 17.
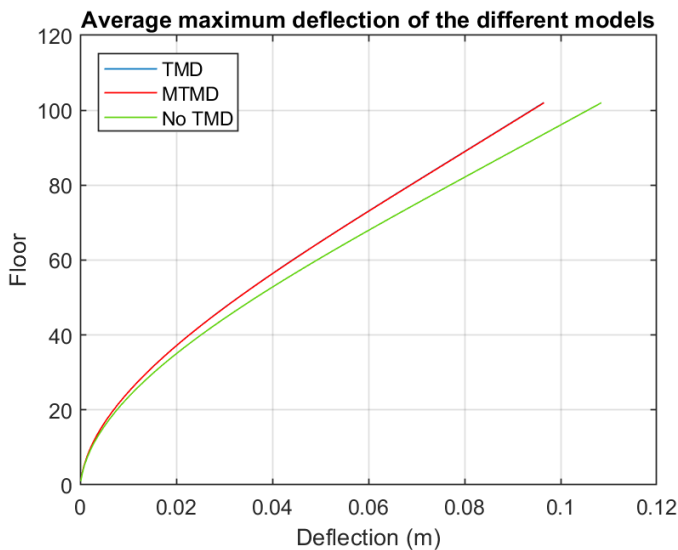

Fig. 17: Average maximum deflection of the different models.

Note that the lines of the TMD system model and the MTMD system model are close together. This will be explained in section V-B1. The average maximum deflection of the top floor of the building models is shown in Table X.

	TMD model	MTMD model	No TMD model
Deflection (m)	0.09644	0.09653	0.1085

TABLE X: Average maximum deflection of the top floor of the building models.

2) Robustness and off-tuning mitigation

In order to determine the robustness and off-tuning mitigation abilities of the MTMD system, the building is off-tuned to the new natural frequencies shown in Table VIII. First, the effect of this off-tuning of the building will be shown. Figure 18 shows a zoomed in version of Figure 15, which is the time response of the MTMD system where the centre TMD system is correctly tuned to the building motion, as can be seen by the fact that the centre TMD system oscillation has a phase difference of exactly $90°$ with respect to the building oscillation.
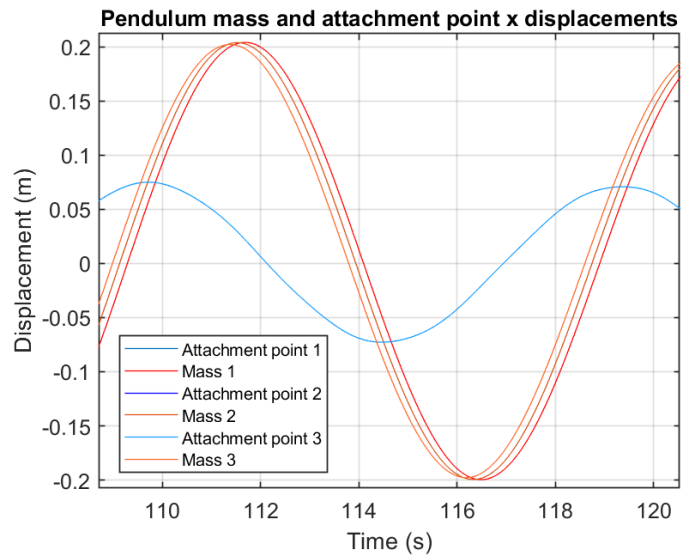

Fig. 18: Zoomed in time response of the MTMD system (zoomed in version of Figure 15).

In Figure 19, a zoomed in version is shown of the time response of the MTMD system where the building is off-tuned to a fundamental natural frequency of $0.1023 Hz$, which causes the centre TMD system to be tuned worse to the building motion, but causes one of the outer TMD systems (pendulum mass 1) to be tuned exactly correct to suppress the building motion. The single TMD system would oscillate at the same location of the centre TMD system (pendulum mass 2). In theory, this means that the MTMD system could suppress the building oscillation more efficiently than the single TMD system, since one of the pendulum MTMD masses is tuned exactly to the off-tuned fundamental natural frequency of the building.
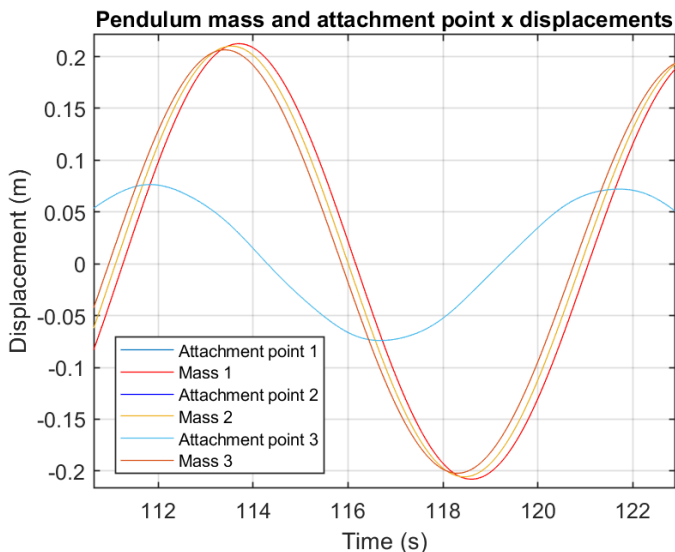
Fig. 19: Zoomed in time response of the MTMD system for an off-tuned building frequency of $0.1023Hz$.

Now, the average maximum deflection of the models is made, as explained before, while using the off-tuned building frequency of $0.1023Hz$. The result is shown in Figure 20.
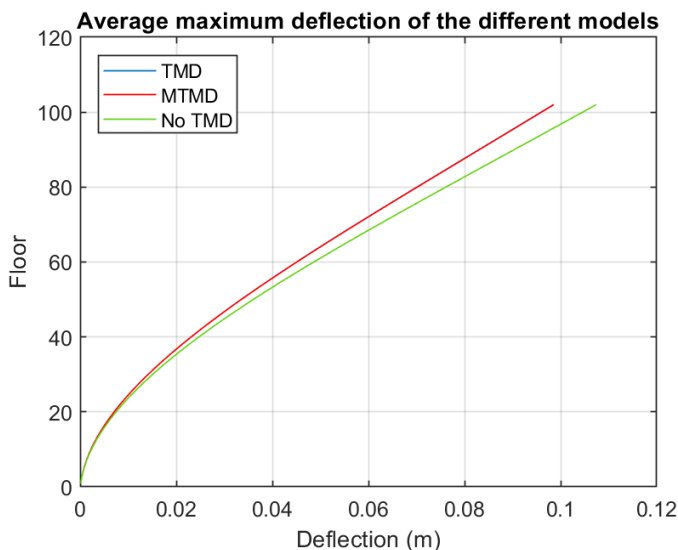

Fig. 20: Average maximum deflection of the different models for an off-tuned building frequency of $0.1023Hz$.

The average maximum deflection of the top floor of the building models is shown in Table XI.

	TMD model	MTMD model	No TMD model
Deflection (m)	0.09851	0.09859	0.1074

TABLE XI: Average maximum deflection of the top floor of the building models, using an off-tuned building frequency of $0.1023Hz$.

3) Space usage

The space usage of the TMD and MTMD systems can be obtained from the actual Taipei 101 building parameters. The single TMD mass of the actual building is $660000kg$. When

taking the total mass of the MTMD system to be equal to this mass, the mass of the three different TMD mass becomes $220000kg$. Taking a density of steel of $7850kg/m^3$, the volume of this mass becomes

$$V = \frac{m}{\rho} = \frac{220000}{7850} = 28.03m^3. \quad (114)$$

Now, the diameter of the mass can be found using

$$V = \frac{4}{3}\pi r^3. \quad (115)$$

Filling in the found volume of $V = 28.03m^3$ and solving for the radius gives $r = 1.884m$, which gives a pendulum mass diameter of $3.769m$. The diameter of the single TMD mass in the actual Taipei 101 building is equal to $5.5m$[37]. The relevant spacial parameters of the TMD and the MTMD systems are shown in Table XII.

	TMD	MTMD
Mass diameter (m)	5.5	3.8
Cable length (m)	42	42
Maximum swing (m)	1.50	1.50

TABLE XII: Relevant spacial parameters of the TMD and MTMD systems.

C. Model behaviour using realistic wind model

The behaviour of the single TMD model is analysed when exposed to a more realistic wind force. Since this is a random wind force, the different models are not compared for this method. However, the simulation of the single TMD system is shown in order to showcase how the building model would behave in more realistic circumstances. The time response of the system is shown in Figure 21.
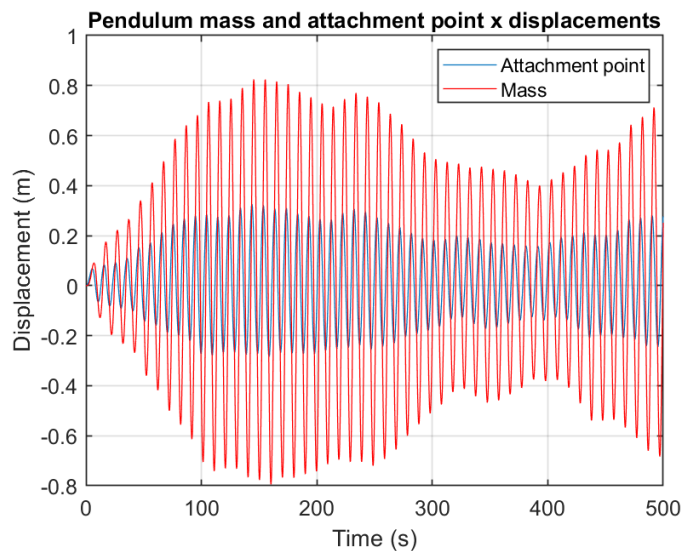

Fig. 21: Time response of the single TMD system, using the realistic wind force model.

The random wind velocity at a height of $15m$ to which the building is exposed is shown in Figure 22.
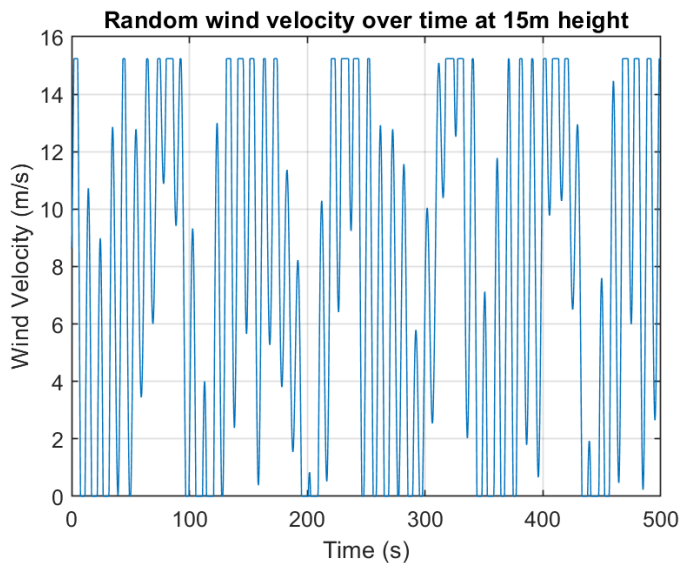
Fig. 22: Wind velocity at a height of $15m$ of the realistic wind model, used for the time response of the single TMD system in Figure 21.

In order to show the influence of the random wind force on the oscillation frequency of the building, a zoomed in version of Figure 21 is shown in Figure 23.
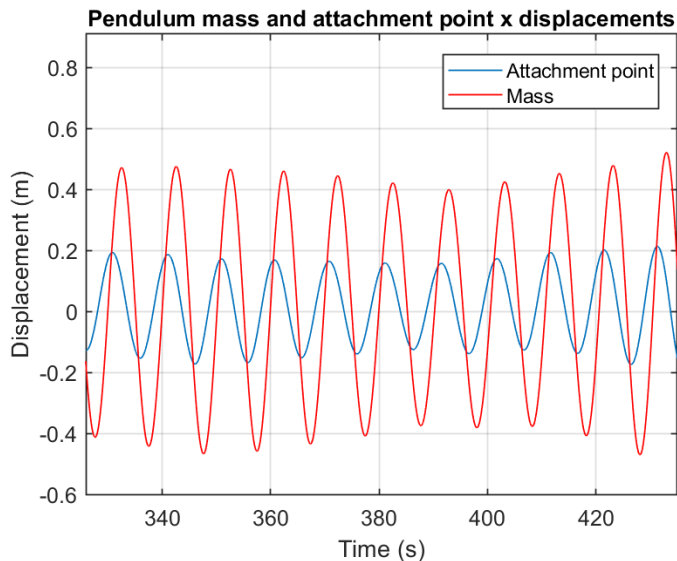

Fig. 23: Zoomed in time response of the single TMD system, using a realistic wind force (zoomed in version of Figure 21).

V. DISCUSSION

In this section, the results of section IV are explained and discussed into detail. Also, potential improvements to the systems, models, analysis techniques or the research project in general are pointed out and discussed.

A. Model validation results

The results of the different methods to validate the behaviour of the building models are discussed in this section.

1) Modal analysis

The mode shapes of the first three modes of the TMD and MTMD models are shown in Figure 10. It can be seen that the modes shapes of both systems are almost identical. This is expected since both building configurations are tuned to roughly the same natural frequencies, as can be seen in Table IX. The biggest difference between the scaled displacement of the TMD and MTMD systems can be found for mode 3, at floor 86, where the difference in scaled displacement between the TMD and MTMD systems is 0.009. When comparing the mode shapes to experimentally determined mode shapes[29], it can be concluded that the first mode of the models accurately represents the first mode of the actual building and that the second and third mode of the models have slightly more displaced mode shapes than the actually building, especially for the lower part of the building. The mode shape of the first mode is the most important to match to the actual building, which is also the case for the eigenfrequencies, which are shown in Table IX. When comparing these eigenfrequencies to the values that are measured[29] for the actual building, it can be concluded that the first mode of the model is slightly too low and that the second and third modes of the model are slightly too high. This is the case because the configuration of the building model was tuned such that all elements were implemented correctly relative to other building elements, based on the implementation of the elements in the actual building. The building dimensions were approximated, after which the mass of the building was determined by taking the pendulum mass to be 0.24% of the building mass and be approximately equal to $660000kg$ at the same time. After this, the eigenfrequencies were tuned to most appropriately match the actual eigenfrequencies. However, the model is constructed based on multiple approximations and simplifications, where the largest simplification is that the building model is made from a truss FEM structure using steel beams. Although such a steel truss structure is present in the actual building, this structure alone does not capture all of the dynamic behaviour of the actual building, where e.g. concrete is used[33] to fill steel columns that are distributed along the building floor plan and that extend along great heights of the building, among many other structural features that are not captured in the simplified truss building model. Although the eigenfrequencies of the building are not exactly matched to the actual eigenfrequencies, the rough building behaviour is represented by the building model. When using these building models to approximate the behaviour of the actual building, it is most important that the different model elements are tuned such that the relative behaviour corresponds to the relative behaviour of the elements in the actual building and the different models are tuned such that a fair comparison can be made. Therefore, although the mode shapes and eigenfrequencies do not exactly match the measured values, adequate results can be obtained about the performance of the different models.

2) Frequency response

The frequency response of all of the nodes of the TMD and MTMD models are shown in Figures 11 and 12. These

figures provide an overview of the dynamic behaviour of the system, which can be compared to the static frequency behaviour resulting from the modal analysis. The visible frequency peaks are located at $0.1040Hz$ and $0.5753Hz$ for both models, where the peak at $0.5753Hz$ is way smaller than the peak as $0.1040Hz$. When comparing the found locations of the frequency peaks to the eigenfrequencies shown in Table IX, it can be seen that the eigenfrequencies of the dynamic system from the frequency response are slightly lower. This is the case because of the Rayleigh damping that is applied to the building. The found damped natural frequencies in the frequency response are thus expected to be slightly lower than the natural frequencies found in the modal analysis, which means that the frequency responses of the models are as expected.

The frequency response shows that the first mode of the building oscillation is by far the most dominant frequency in the system. This means that tuning some TMD systems in the MTMD system to the second mode of vibration does not have much influence on the suppression of the building vibration.

3) Small angle approximation

The small angle approximation validation result is shown in Figure 13. It is assumed that the maximum wind force that the building will ever be exposed to is equal to $32.78m/s$[38]. The maximum pendulum angle θ that the building will have when this wind velocity is present, for a pendulum damping of $\zeta_p = 0.30$, is found to be $\theta = 0.0328rad$, as can be seen in Figure 13 at a time of $t = 25.50s$. The small angle approximation is used for the pendulum equations in the model, such that

$$\sin(\theta) \approx \theta. \tag{116}$$

For this approximation to be accurate, the pendulum angle θ should be small, where the approximation is more accurate for smaller angles. However, as a rule of thumb, the approximation is considered to be valid when θ satisfies the relation

$$\theta < 0.1rad, \tag{117}$$

which is equivalent to

$$\theta < 5.73°. \tag{118}$$

Therefore, since the maximum pendulum angle that will ever occur is equal to $\theta = 0.0328rad$, the small angle approximation is valid.

B. Model comparison results

The results of the different methods to compare the behaviour of the building models are discussed in this section.

1) Suppression ability

The suppression abilities of the different models is shown in two different ways. First a time response of all of the three models is shown in Figures 14, 15 and 16. It can be seen that all of the time responses converge to the equilibrium position, since damping is applied to the building and pendulum.

However, it is clearly visible that the attachment points of the TMD and MTMD systems and thus the building in general converges to the equilibrium point faster than the system without a TMD installed. The difference between the TMD and MTMD systems is not clearly visible using this analysis method, which is why a second analysis method is introduced.

For this second analysis method, the average maximum deflection is plotted, as explained before. This average maximum deflection is shown in Figure 17. In this figure, it can also be seen clearly that the 'no TMD' system has a higher deflection than the TMD and the MTMD systems. Also, it can be seen more clearly how close the TMD system and MTMD system are together. The deflections of the top floor of the different models are shown in Table X. From these values can be concluded that the TMD system performes slightly better than the MTMD system. This is as expected, since for the TMD system, the entirety of the pendulum mass is tuned to the frequency of the building, while for the MTMD system, the outer masses are not exactly tuned to this frequency, resulting in slightly less anti-resonance and thus slightly less vibration mitigation for the MTMD system, which is expected for this situation where the pendulums are tuned to the building oscillation frequency.

2) Robustness and off-tuning mitigation

The robustness and off-tuning mitigation performance of the MTMD system is analysed by tuning the building oscillation frequency to $0.1023Hz$ instead of $0.1043Hz$ and keeping the pendulum systems tuned as before. This means that the single TMD system is off-tuned slightly, as well as the centre TMD of the MTMD system. However, for the MTMD system, one of the outer masses (mass 1) is now tuned correctly to the building frequency. This difference in tuning of the TMD systems for the initial building frequency and the off-tuned building frequency is shown in Figures 18 and 19 respectively.

Now, in order to determine the performance of the MTMD system with respect to the TMD system for the off-tuned building frequency, the average maximum deflection is determined for this situation, which is shown in Figure 20. It is clear that both the TMD and MTMD system still provide better vibration suppression than the 'no TMD' system. However, in Table XI can be seen that the MTMD system does not outperform the single TMD system when it comes to the average maximum deflection of the top floor of the building, even though the MTMD model has a mass that is tuned exactly to the off-tuned building frequency. This confirms the result that was found in the second parameter sweep in section III-E2, which is that introducing a bandwidth to the MTMD system does not improve the suppression abilities of the system, but instead makes the suppression abilities slightly worse. Therefore, according to the results of the model, it is not beneficial to have an MTMD system which provides a vibration suppression bandwidth, which has the same total mass of a single TMD system, whether the pendulums are tuned exactly to the building frequency or are slightly off-tuned. This conclusion

is very reductive and should involve many more insights and considerations. A more complete conclusion is given in section VI, where various explanations for the results are elaborated.

3) Space usage
When comparing the spacial parameters of the TMD and MTMD systems shown in Table XII, it can be seen that the cable lengths of the models are chosen to be the same. This is because the natural frequencies of the TMD masses in the MTMD system are tuned using the rotational spring constant k. In the actual system this would mean that the masses would be tuned by changing the stiffness of springs that would be attached to the pendulum mass. Another method of changing the pendulum frequency would be to change the cable length of the different pendulums, which would make some of the cable lengths of the masses in the MTMD system larger than for the single TMD system and some of the cable lengths smaller. For this analysis, it is assumed that the pendulums of the MTMD system are tuned using springs. This makes the lengths of all of the cables both models equal, which means that the different systems require the same amount of vertical space.

In the MTMD model, the three pendulums are tuned such that the maximum swing is $1.50m$, which is the same as is taken for the single TMD mass. This would mean that the MTMD system needs exactly three times as much space as the single TMD system, because the space that the single TMD system requires is used three times. If this maximum swing would be reduced for the masses of the MTMD system, proportional to the reduction in diameter of the masses, then the maximum swing of the masses in the TMD system would be $1.50/5.5 \cdot 3.8 = 1.04m$. The maximum swing is defined as a radius from the equilibrium point, which means that the mass can swing as far as the maximum swing in all horizontal directions. Even with this proportional reduction in maximum swing, the horizontal area of this swing would require $1.04^2 \cdot \pi = 3.37m^2$, which is $10.12m^2$ for three pendulum masses in the total MTMD system. For the single TMD system, the required horizontal area for the swing is $1.50^2 \cdot \pi = 7.06m^2$. This means that the horizontal space required by the MTMD system is more than the horizontal space required by the TMD system.

In general it can be concluded that the MTMD pendulum system requires more space than the TMD pendulum system. Additionally, the space required would not be concentrated at a single location, which means that multiple locations in the building would have to be constructed such that $42m$ long cables can be attached, which means that this space would be occupied in more locations. Although the required space per mass of the MTMD system would be lower than for the single TMD system, the total required space would be higher. Also, multiple systems would have to be constructed, which includes the construction of more damper systems, more pendulum cables and more frame work to which the masses can be attached.

C. Model behaviour using realistic wind model
The behaviour of the single TMD model under the influence of a more realistic wind model is shown in Figure 21. The applied wind velocity at a height of $15m$ is shown in Figure 22. It can be seen that the time response is not symmetric in the x-axis, which is logical, not only because of the random wind force, but also because the wind force is only coming from the left side of the building. This also causes the displacement of the building to be slightly more towards the right side (positive y-direction) then to the left side (negative y-direction).

In Figure 23 can be seen that the oscillation frequency of the building is slightly affected by the applied random wind load. This causes the TMD mass to be slightly off-tuned for some periods of time (around $t = 380s$ in Figure 23) and to be correctly tuned at other moments (around $t = 0s$ and $t = 430s$ in Figure 23). Theoretically, this would make the implementation of an MTMD system better, since the various MTMD systems could be tuned to cover this range in which the building frequency can be slightly off-tuned due to influence of the external wind forces. However, as shown and discussed in sections IV-B2 and V-B2, the MTMD system does not provide better suppression abilities than the single TMD system for this building configuration.

D. Potential improvements
The research project provides clear results about the performance in simulation of TMD and MTMD systems in the Taipei 101 building. This will be elaborated upon in section VI. In this section, potential improvements to the models and errors in the modelling or analysis will be mentioned and discussed.

1) Internal building damping
After the analysis of the simulations, it was found that the internal building damping was not calculated correctly initially. The mistake was made that the frequency of the building (in Hz) was filled in in Eq. (38) for the angular frequency, without converting the frequency to angular frequency using Eq. (39). This was the only found error in the model and analysis calculations. However, this resulted in a smaller required value for α of $\alpha = 0.003431$, which means that the buildings in the simulation are damped less than the actual building. However, although this causes the displacement of the building to differ from the actual building displacement, since the same calculation error was made in the TMD, MTMD and 'no TMD' models, this error was not considered to affect the comparison of the performance of the different models.

2) Model simplifications
As discussed in section III-B, the building model is made using assumptions and approximations in order to most accurately represent the Taipei 101 building, while still being able to compute the dynamical building behaviour over time in a reasonable amount of time. This results in

simplifications of the building structure, where a steel truss structure is used to represent the entire building. Although a steel truss structure is present in the actual building, all of the other materials and constructions, such as concrete filled steel columns as described in section V-A1, contribute to the dynamic behaviour of the building, making it different than the dynamic behaviour of the model.

Also, the building shape differs from the actual building shape, where a rectangular structure is used to represent the actual building, which mainly consists of multiple units where the floor area increases with the increase in height. Also, the bottom part of the building is wider than the main part of the building, which consists of the units as explained above. This configuration can be seen in Figure 1. In the building model, the average dimensions of the main part of the building are taken as the dimensions of the rectangular structure shown in Figure 24. This means that the width of the building model is larger than the width of the actual building at some locations and smaller at other locations, depending on the building height. This average was taken to approximate the building structure. In order to make the dynamic behaviour of the building models even more accurate, the building structure could be represented more accurately. Also, the height of the structure in the building model was taken to be $448m$, since this is the height of the actual building up to the top floor. For the actual building, a pinnacle is located on top of the building, which increases the total building height to $508m$[29]. This pinnacle structure, including two extra relatively small TMD systems, is not included in the building model.

In Figure 24 can be seen that there are 50 floors taken into account in the building model instead of 101. Therefore, it might seem that the building is only half as high as the Taipei 101 building. However, because the height of the building is chosen to correspond to the actual building height, each of the floors in the building model represents 2 floors in the actual building. This means that the vertical beam elements in the model have a length of two times the height of one floor. This means that the beam elements are slightly longer, which makes the Euler-Bernoulli beam theory more valid, due to the relatively high cross-sectional area of the beam elements, as shown in Table II.

3) Energy conservation

The behaviour of the different models was validated and compared using multiple analysis methods. One additional validation method could be applied, which is checking the energy conservation of the system. When no damping is applied to the system, the total energy of the system should remain the same over time during the dynamic simulation, since without damping there is no way for the energy to be dissipated. The total energy of the system should be equal to the kinetic energy of the building (T), summed with the strain energy of the building (V), the kinetic energy of the pendulum (T_p) and the potential energy of the pendulum (V_p), which

gives

$$E_{tot} = T + V + T_p + V_p, \tag{119}$$

where E_{tot} is the total energy of the building and the other terms are equal to[32]

$$T = \frac{1}{2}\dot{\mathbf{u}}^T \mathbf{M}\dot{\mathbf{u}}, \tag{120}$$

$$V = \frac{1}{2}\mathbf{u}^T \mathbf{K}\mathbf{u}, \tag{121}$$

$$T_p = \frac{1}{2}mL^2\dot{\theta}, \tag{122}$$

$$V_p = mgL(1 - \cos\theta). \tag{123}$$

The individual terms of Eq. (119) would differ over time during the dynamic building simulation, but the total energy should remain constant. This analysis method could be used to further validate the models.

4) Attachment point locations and amount of MTMD masses

Using the results of the first parameter sweep of section III-E2, it was concluded that the MTMD system performed best when the three systems were placed as high in the building as possible. This study was limited to only consider the situation where the attachment points of the masses of the three systems were located at an equal building height, at horizontal locations of $\frac{1}{6}L_w$, $\frac{1}{2}L_w$ and $\frac{5}{6}L_w$, where L_w is the width of the building, because this would provide symmetry in the building structure. However, a more thorough study can be performed regarding the location of the attachment points of the masses of the MTMD system, in order to determine whether this could influence the performance of the system. For example, the individual masses in the MTMD system can be attached at different heights of the building or at different horizontal locations. Also, more masses could be added to the MTMD system, which could all be tuned slightly differently, to obtain a bandwidth of the MTMD system that transitions more smoothly around the centre frequency.

VI. CONCLUSION

It can be concluded according to the different building models, that the MTMD system does not provide a better suppression ability than the single TMD system, when the building is off-tuned to a slightly different fundamental natural frequency, due to temporary weather circumstances or permanent changes to the building structure. The performance of both systems is almost identical with the used bandwidth of $0.1023Hz - 0.1063Hz$ for the MTMD system in this study, where the building is off-tuned from the initial fundamental natural frequency of $0.1043Hz$ to a frequency of $0.1023Hz$. However, it was concluded that the TMD system performs slightly better, also for the situation where the fundamental natural frequency of the building is not off-tuned and is equal to $0.1043Hz$. Additionally, the space usage of the single TMD system was found to be more efficient than the space usage of the MTMD system. Considering all of the obtained results of the performed analysis methods, it can be concluded that a single

TMD system is preferred over an MTMD system, in terms of suppression ability, robustness, off-tuning mitigation and space usage, when using a building configuration as described in this study. However, in the MTMD model used in this study, the frequency bandwidth is equally distributed around the centre frequency. It was found that both the TMD and MTMD systems perform better when tuned to the correct fundamental natural frequency of the building, but that the difference between these systems is almost negligible when the centre frequency of the MTMD system is tuned to the same frequency to which the single TMD system is tuned. If it could be predicted in which direction the fundamental natural frequency of the building would change over time, the masses of the MTMD system could be tuned such that a bandwidth is obtained that is not centred around the initial fundamental natural frequency of the building. Although this could provide better performance of the MTMD system during short- and long-term changes in fundamental natural frequency of the building, for long-term (permanent) changes, for which the frequency of the system does not have to change frequently but instead slowly over time, the same frequency bandwidth can be obtained by implementing a single TMD system of which the length of the pendulum cables can be modified to a certain extent. It should be noted that the results of this study are limited to certain approximations and assumptions, as discussed in sections III-B and V-D. Improvements that make the model or analysis methods more extensive or accurate could potentially lead to different results. More system configurations can be examined in order to further validate the obtained results or to disprove the results of this study.

VII. FURTHER RESEARCH

In this research project, an analysis is conducted on the performance of a single TMD system and an MTMD system, which are located in a wind-excited building. When considering wind forces, the building experiences increasingly larger forces at higher locations on the building, due to the increasing wind velocity with height. This means that a large amount of the force acting on the building is applied on the higher levels of the building. Apart from strong winds and typhoons, earthquakes occur frequently around the Taipei 101 building. When earthquakes occur, the resulting force is distributed in a different way than for wind gusts. Although earthquakes also induce movement of the building, the forces are applied at the bottom of the building, since the ground vibrations cause the building to start moving. This would give a different building response and potentially lead to different requirements for TMD systems that are installed in the building. Determining the suppression abilities of the TMD and MTMD systems for both wind forces and seismic activity could lead to improvements that make the system more suitable to mitigate building vibrations due to both wind gusts and earthquakes, which makes it worthwhile to investigate the influence of this type of external force as well.

Additionally, the implementation of multiple linear TMD systems could be considered, instead of multiple pendulum TMD systems. It is found that the pendulum MTMD system occupies more space than the single pendulum TMD system, even when the total mass of the two systems is the same. A pendulum TMD system needs a substantial amount of space due to the pendulum cables with which the mass is attached. These cables need to be relatively long in order to be the correct length for the TMD system to be tuned to the oscillation frequency of the building. Also, the pendulum mass in the Taipei 101 building has the shape of a sphere, which is a logical shape for a pendulum mass, but not a convenient shape in terms of space usage. However, when considering a linear TMD system, the required space of the system could potentially be reduced, by placing the masses in more convenient places, where the masses can also be shaped more conveniently. For example, linear TMD systems could be implemented inside of floors and walls, which provides more practical spacing of the MTMD system. Research could be performed to examine whether the implementation of these linear TMD systems in a practical configuration, such as implementation inside of floors and walls, would improve the space usage of the MTMD system, while also having the ability to provide an equal or improved vibration mitigation.

VIII. ACKNOWLEDGEMENTS

REFERENCES

[1] F. Rahimi, R. Aghayari, and B. Samali, "Application of tuned mass dampers for structural vibration control: A state-of-the-art review," *Civil Engineering Journal*, vol. 6, 8 2020. DOI: 10.28991/cej-2020-03091571.

[2] J. Wang and C. Lin, "Extracting parameters of tmd and primary structure from the combined system responses," *Smart Structures and Systems*, vol. 16, pp. 937–960, 5 2015. DOI: 10.12989/sss.2015.16.5.937.

[3] F. Sadek, B. Mohraz, A. Taylor, and R. Chung, "A method of estimating the parameters of tuned mass dampers for seismic applications," *Earthquake Engineering Structural Dynamics*, vol. 26, pp. 617–635, 6 1998. DOI: 10.1002/(SICI)1096-9845(199706)26:6⟨617::AID-EQE664⟩3.0.CO;2-Z.

[4] L. Chung, L. Wu, C. Yang, K. Lien, M. Lin, and H. Huang, "Optimal design formulas for viscous tuned mass dampers in wind-excited structures," *Structural Control and Health Monitoring*, vol. 20, pp. 320–336, 3 2011. DOI: 10.1002/stc.496.

[5] M. Soto and H. Adeli, "Tuned mass dampers," *Archives of Computational Methods in Engineering*, vol. 20, pp. 419–431, 2013. DOI: 10.1007/s11831-013-9091-7.

[6] R. Yogesh, S. Suryawanshi, A. Shitole, and T. Rahane, "Study of tuned mass dampers system as vibration controller in multistoried buildings," *International Journal of Advanced and Innovative Research*, vol. 1, pp. 280–284, 2012.

[7] C. Chang and H. Yang, "Control of buildings using active tuned mass dampers," *Journal of Engineering Mechanics*, vol. 121, 3 1995. DOI: 10.1061/(ASCE) 0733-9399(1995)121:3(355).

[8] C. Li and Y. Liu, "Active multiple tuned mass dampers for structures under the ground acceleration," *Earthquake Engineering Structural Dynamic*, vol. 31, pp. 1041–1052, 5 2002. DOI: 10.1002/eqe.136.

[9] L. Chung, Y. Lai, C. Yang, K. Lien, and L. Wu, "Semi-active tuned mass dampers with phase control," *Journal of Sound and Vibration*, vol. 332, pp. 3610–3625, 15 2013. DOI: 10.1016/j.jsv.2013.02.008.

[10] Y. Chen, P. Guéguen, K. Chen, *et al.*, "Dynamic characteristics of taipei 101 skyscraper from rotational and translation seismometers," *Bulletin of the Seismological Society of America*, vol. 113, pp. 690–709, 2 2023. DOI: 10.1785/0120220147.

[11] H. Gao, C. Wang, C. Huang, W. Shi, and L. Huo, "Development of a frequency-adjustable tuned mass damper (fatmd) for structural vibration control," *Shock and Vibration*, vol. 2020, 1 2020. DOI: 10.1155/2020/9605028.

[12] C. Lee, Y. Chen, L. Chung, and Y. Wang, "Optimal design theories and applications of tuned mass dampers," *Engineering Structures*, vol. 28, pp. 43–53, 1 2006. DOI: 10.1016/j.engstruct.2005.06.023.

[13] G. Lin, C. Lin, T. Yang, and H. Lung, "Experimental verification of seismic vibration control of high-rise buildings with friction-type multiple tuned mass dampers," *Engineering Structures*, vol. 302, 2024. DOI: 10.1016/j.engstruct.2023.117401.

[14] M. Abé and Y. Fujino, "Dynamic characterization of multiple tuned mass dampers and some design formulas," *Earthquake Engineering Structural Dynamics*, vol. 23, pp. 813–835, 8 1994. DOI: 10.1002/eqe.4290230802.

[15] J. Park and D. Reed, "Analysis of uniformly and linearly distributed mass dampers under harmonic and earthquake excitation," *Engineering Structures*, vol. 23, pp. 802–814, 7 2001. DOI: 10.1016/S0141-0296(00)00095-X.

[16] K. Xu and T. Igusa, "Dynamic characteristics of multiple substructures with closely spaced frequencies," *Earthquake Engineering Structural Dynamics*, vol. 21, pp. 1059–1070, 12 1992. DOI: 10.1002/eqe.4290211203.

[17] H. Yamaguchi and N. Harnpornchai, "Fundamental characteristics of multiple tuned mass dampers for suppressing harmonically forced oscillations," *Earthquake Engineering Structural Dynamics*, vol. 22, pp. 51–62, 1 1993. DOI: 10.1002/eqe.4290220105.

[18] C. Li, "Performance of multiple tuned mass dampers for attenuating undesirable oscillations of structures under the ground acceleration," *Earthquake Engineering Structural Dynamics*, vol. 29, pp. 1405–1421, 9 2000. DOI: 10.1002/1096-9845(200009)29:9⟨1405::AID-EQE976⟩3.0.CO;2-4.

[19] C. Li and Y. Liu, "Ground motion dominant frequency effect on the design of multiple tuned mass dampers," *Journal of Earthquake Engineering*, vol. 8, pp. 89–105, 1 2008. DOI: 10.1080/13632460409350482.

[20] C. Li and Y. Liu, "Optimum multiple tuned mass dampers for structures under the ground acceleration based on the uniform distribution of system parameters," *Earthquake Engineering Structural Dynamics*, vol. 32, pp. 671–690, 5 2003. DOI: 10.1002/eqe.239.

[21] D. Caicedo, L. Lara-Valencia, J. Blandon, and C. Graciano, "Seismic response of high-rise buildings through metaheuristic-based optimization using tuned mass dampers and tuned mass dampers inerter," *Journal of Building Engineering*, vol. 34, 2021. DOI: 10.1016/j.jobe.2020.101927.

[22] S. Suthar and P. Banerji, "Inerter-assisted pendulum-tuned mass damper for across-wind response control of tall buildings," *Engineering Structures*, vol. 291, 2023. DOI: 10.1016/j.engstruct.2023.116489.

[23] P. Brzeski, E. Pavlovskaia, T. Kapitaniak, and P. Perlikowski, "The application of inerter in tuned mass absorber," *International Jounral of Non-Linear Mechanics*, vol. 70, pp. 20–29, 2015. DOI: 10.1016/j.ijnonlinmec.2014.10.013.

[24] A. Giaralis and F. Petrini, "Wind-induced vibration mitigation in tall buildings using the tuned mass-damper-inerter (tmdi)," *Journal of Structural Engineering*, vol. 143, 9 2017. DOI: 10.1061/(asce)st.1943-541x.0001863.

[25] J. Dai, Z. Xu, and P. Gai, "Tuned mass-damper-inerter control of wind-induced vibration of flexible structures based on inerter location," *Engineering Structures*, vol. 199, 2019. DOI: 10.1016/j.engstruct.2019.109585.

[26] Q. Wang, H. Qiao, D. Domenico, Z. Zhu, and Z. Xie, "Wind-induced response control of high-rise buildings using inerter-based vibration absorbers," *Applied Sciences*, vol. 9, p. 5054, 23 2019. DOI: 10.3390/app9235045.

[27] A. Tuan and G. Shang, "Vibration control in a 101-storey building using a tuned mass damper," *Journal of Applied Science and Engineering*, vol. 17, pp. 141–156, 2 2014. DOI: 10.6180/jase.2014.17.2.05.

[28] L. Chung, L. Wu, H. Huang, C. Chang, and K. Lien, "Optimal design theories of tuned mass dampers with nonlinear viscous damping," *Earthquake Engineering and Engineering Vibration*, vol. 8, pp. 547–560, 2009. DOI: 10.1007/s11803-009-9115-3.

[29] Q. Li, L. Zhi, A. Tuan, C. Kao, S. Su, and C. Wu, "Dynamic behavior of taipei 101 tower: Field measurement and numerical analysis," *Journal of Structural Engineering*, vol. 137, 1 2011. DOI: 10.1061/(ASCE) ST.1943-541X.0000264.

[30] K. Chen, J. Wang, B. Huang, C. Liu, and W. Huang, "Vibrations of the taipei 101 skyscraper caused by the 2011 tohoku earthquake, japan," *Earth, Planets and Space*, vol. 64, pp. 1277–1286, 2012. DOI: 10.5047/eps.2012.04.004.

[31]   R. Lewis, "Taipei 101," *Britannica*, 2024. [Online]. Available: https://www.britannica.com/place/Taipei-101.

[32]   R. Craig, *Structural Dynamics: An Introduction to Computer Methods*. John Wiley Sons, 1981, ISBN: 9780471044994.

[33]   D. Poon, S. Shieh, L. Joseph, and C. Chang, "Structural design of taipei 101, the world's tallest building," Seoul, Korea: Council on Tall Building and Urban Habitat, October 10-13 2004.

[34]   P. Ghavami, "Mechanics of materials: An introduction to engineering technology," *Springer International Publishing*, pp. 111–141, 2014. DOI: 10.1007/978-3-319-07572-3_5.

[35]   The Engineering ToolBox, "Young's modulus, tensile strength and yield strength values for some materials," 2003. [Online]. Available: https://www.engineeringtoolbox.com/young-modulus-d_417.html.

[36]   The Engineering ToolBox, "Metals and alloys - densities," 2004. [Online]. Available: https://www.engineeringtoolbox.com/metal-alloys-densities-d_50.html.

[37]   Taipei 101, "Observatory feature," 2019. [Online]. Available: https://www.taipei-101.com.tw/en/observatory/feature.

[38]   National Weather Service - National Oceanic and Atmospheric Administration, "Beaufort wind scale," 2024. [Online]. Available: https://www.weather.gov/mfl/beaufort.

[39]   N. Newmark, "A method of computation for structural dynamics," vol. 85, 3 1959. DOI: 10.1061/JMCEA3.0000098.

[40]   X. Wang, Z. Yao, Y. Guo, and Y. Li, "Analysis of the near-ground wind field characteristics during typhoon soulik," *Applied Sciences*, vol. 14, p. 4001, 10 2024. DOI: 10.3390/app14104001.

[41]   F. Bañuelos-Ruedas, C. Angeles-Camacho, and S. Rios-Marcuello, "Methodologies used in the extrapolation of wind speed data at different heights and its impact in the wind energy resource assessment in a region," *Wind Farm - Technical Regulations, Potential Estimation and Siting Assessment*, 2011. DOI: 10.5772/20669.

[42]   C. Jung and D. Schindler, "The role of the power law exponent in wind energy assessment: A global analysis," *International Journal of Energy Research*, vol. 45, pp. 8484–8496, 6 2020. DOI: 10.1002/er.6382.
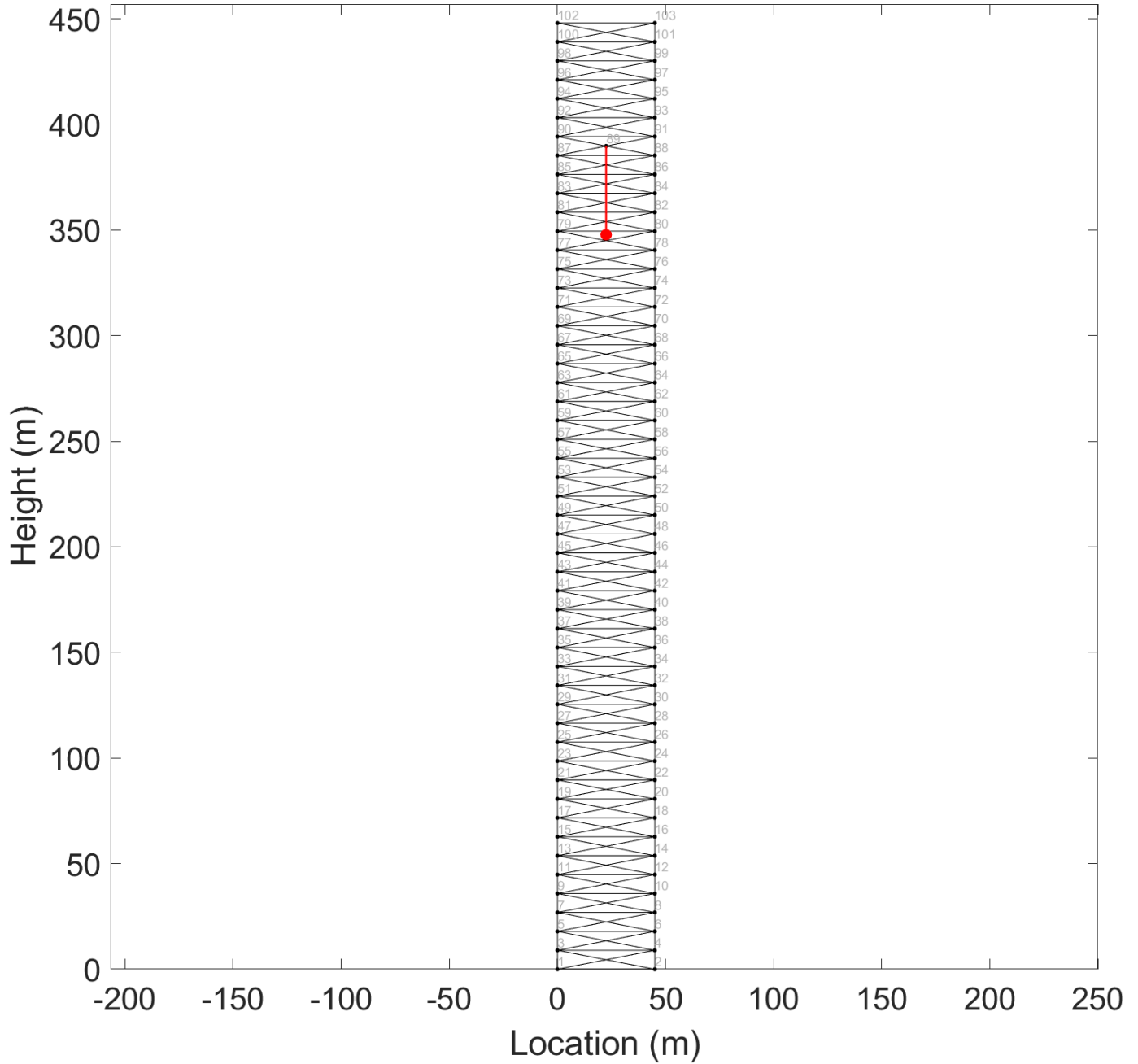
IX. Appendix

Single TMD system static building model

Fig. 24: Single TMD system static building model